Ore Geology Reviews 88 (2017) 370–383

Contents lists available at ScienceDirect

Ore Geology Reviews

journal homepage: www.elsevier.com/locate/oregeo

Adakite-like signature of porphyry granitoid stocks in the Meiduk and Parkam porphyry copper deposits, NE of Shahr-e-Babak, Kerman, Iran: Constrains on geochemistry

Ali Alirezaei *, Mohsen Arvin, Sara Dargahi

Department of Geology, Shahid Bahonar University of Kerman, P.O. Box 76175-133 Kerman, Iran

ARTICLE INFO

Article history:
Received 3 January 2016
Received in revised form 14 April 2017
Accepted 24 April 2017
Available online 27 April 2017

Keywords:
Urumieh-Dukhtar belt
I-type granitoids
Post-collisional tectonic setting
Adakite
Crustal thickening

ABSTRACT

The Middle Miocene porphyry granitoid stocks of Meiduk and Parkam porphyry copper deposits are intruded in the north-western part of the Dehaj-Sarduiyeh volcano-sedimentary belt in the south-eastern extension of the Urumieh-Dukhtar Magmatic Arc (UDMA) in Iran. The porphyritic to microgranular granitoids are mainly consist of quartz diorite, granodiorite and diorite. The whole rock geochemical analyses of these rocks reveals sub-alkaline, calc-alkaline, meta-peraluminous and I-type characteristics. Their geochemical characteristics such as Al_2O_3 content of 13.51–17.05 wt%, high Sr concentration (mostly >400 ppm), low Yb (an average of 0.74 ppm) and Y (an average of 9.02 ppm) contents, strongly differentiated REE patterns ($La/Yb \geq 20$), lack of Eu anomaly ($Eu/Eu^* \geq 1$) are indicative of adakitic signature. Their enrichment in low field strength elements (LFSE) and conspicuous negative anomalies for Nb, Ta and Ti are typical of subduction related magmas. Detailed petrological studies and geochemical data indicated that Meiduk and Parkam porphyry granitoids were derived from amphibole fractionation of hydrous melts at a depth of >40 km in a post-collisional tectonic setting.

1. Introduction

Adakite is a petrological term, first described by Kay (1987) who studied magnesian andesites from the Adak Island of the Aleutian mountain chain, Alaska. He used the term adakite for rocks with specific geochemical features and tectonic history. The formation of adakitic magma was originally attributed to the melting of young and hot oceanic crust (Kay, 1987; Green and Harry, 1999; Defant and Drummond, 1990). However, such magmas were also reported from, continental arc, mature volcanic arc and post-collisional tectonic settings (Rapp et al., 1999; Atherton and Petford, 1993; Whattam et al., 2012; Petford and Atherton, 1996). In addition, adakitic like features were recognized in the porphyritic intrusions associated with porphyry copper deposits (Stern and Skewes, 2005; Han et al., 2006; Mungall, 2002; Oyarzun et al., 2001; Li et al., 2011; Loucks, 2014; Lu et al., 2015, 2016). Copper-ore-forming adakitic magmas are hydrous and oxidized, enriched in sulphur and metal that are needed for the formation of porphyry copper deposits (Burnham, 1979; Loucks, 2014). It was suggested that the amount of water required for copper mineralization during the Melting-Assimilation-Storage-Homogenization (MASH) process can be attributed either to the ascent of hydrous magma from melting of mantle lithosphere (Lu et al., 2015), melting of remnants of previous arc magmatism at plates collision or through the breakdown of amphibole in the lower parts of thickened continental crust (Richards, 2003, 2009; Hou et al., 2015a,b). Magmas that are produced by melting of mantle wedge in the subduction zones have volatile materials, copper and sulphur for the formation of porphyry copper deposits (Richards, 2003). The compressional conditions together with oxidized nature of adakitic magma can dissolve large amounts of sulphide in the source region and adding it into the melt, transferring of sulphides in the magma and preventing separation of sulphide phases from intermediate-felsic melt. The ascent of this hydrous, oxidized sulphur and metal rich magma and its emplacement into shallow depth in the crust can be related to formation of large porphyry copper deposits (Richards, 2003; Wang et al., 2006; Rohrlach and Loucks, 2005).

Some aspects of economic feasibility, mineralization processes, metallogeny, dating, and mineral chemistry in the Meiduk porphyry copper deposit were further discussed by Outomec (1992), Hassanzadeh (1993) and Asadi et al. (2013). The supergene enrichment zone, approximately 50 m thick, is one of the main sources of Cu ore. The proved reserve at Meduk is 180Mt@0.8% Cu, while the Pakram is at moment sub-economic showing an average copper

* Corresponding author.
E-mail address: ali.alirezaei.ir@gmail.com (A. Alirezaei).

http://dx.doi.org/10.1016/j.oregeorev.2017.04.023
0169-1368/

grade of 0.22% . The proved reserve at the Sarcheshmeh porphyry copper deposit, located 85 km southeast of the Meiduk, is 1200 Mt@0.69% Cu and 0.03% Mo (Shahabpour, 2000).

The main aim of this research is to use whole rock geochemistry in order to provide new constraints on the formation and tectono-magmatic evolution of the host adakite-like granitoids of the Meiduk and Parkam porphyry copper deposits.

2. Geological setting

The Zagros mountain chain is part of the Alpine-Himalayan orogenic belt and structurally is subdivided into Zagros Folded and Thrust Belt, Zagros Suture Zone, Sanandaj-Sirjan Zone and Urumieh-Dukhtar Magmatic Arc (UDMA) (Berberian and King, 1981; Alavi, 1994, 2004; Mohajjel and Fergusson, 2000) (Fig. 1). These structural zones are related to the continuous subduction of the Neo-Tethys ocean for most of the Mesozoic and Cenozoic time under the southern margin of the Central Iranian plate along the thrust of the Zagros which eventually led to the collision of the Arabian plate with the Iranian plate in the Late Eocene time (Berberian et al., 1982; Hempton, 1987; Beydoun et al., 1992; Ricou, 1994; Mohajjel et al., 2003; Agard et al., 2005; Alavi, 2007; Allen and Armstrong, 2008; Dragahi et al., 2008; Horton et al., 2008). The subduction led to extensive volcanic activities in the Eocene-Oligocene time along the UDMA. The distinctive south-eastern part of the UDMA which is known as the Dehaj-Sarduiyeh volcano-sedimentary belt hosts two significant types of granitoids (Jebale-Barez and Kuh-Panj). The Jebale-Barez granitoids emplaced in deep crustal level in the Middle Eocene-Oligocene, whereas the Kohe-Panj hypabyssal type granitoids emplaced after the end of subduction in the Middle-Upper Miocene (Berberian et al., 1982; Mohajjel et al., 2003; Alavi, 2007; Dargahi, 2007). The Kuh-Panj granitoid plutons host large porphyry copper deposits such as Sarcheshmeh and Meiduk and less significant Parkam in the study area (Fig. 1). The Meiduk and

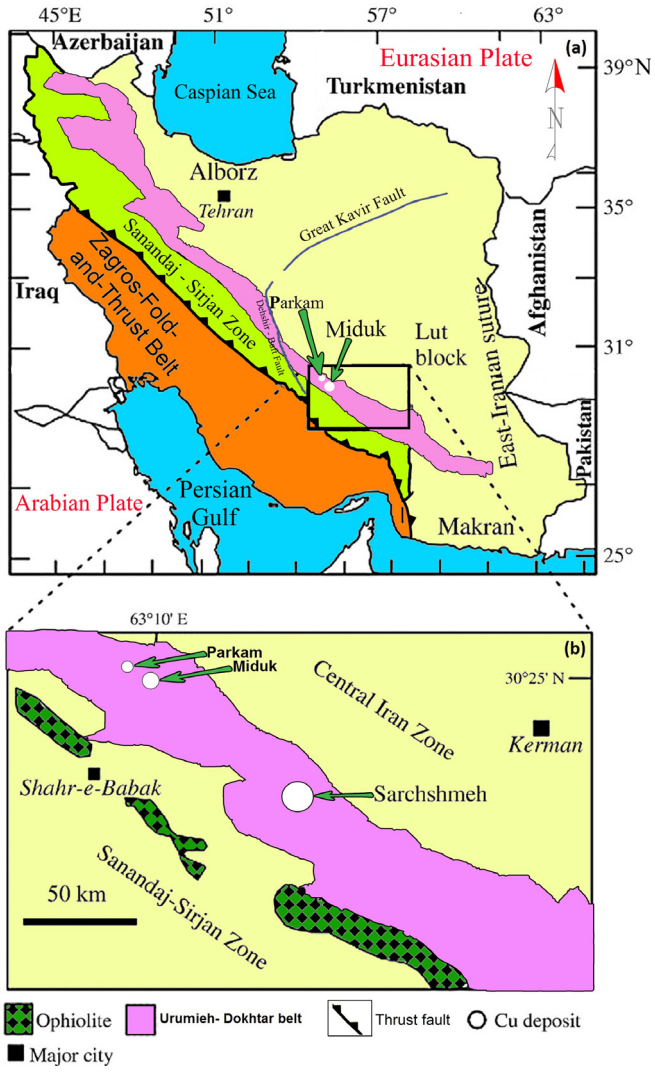

Fig. 1. (a) Map showing major litho-tectonic structural zones of Iran (Modified after Berberian and King, 1981; Asadi et al., 2015). (b) The location of the Meiduk and Parkam porphyry copper deposits in the Dehaj-Sarduiyeh belt (Modified after Berberian and King, 1981).

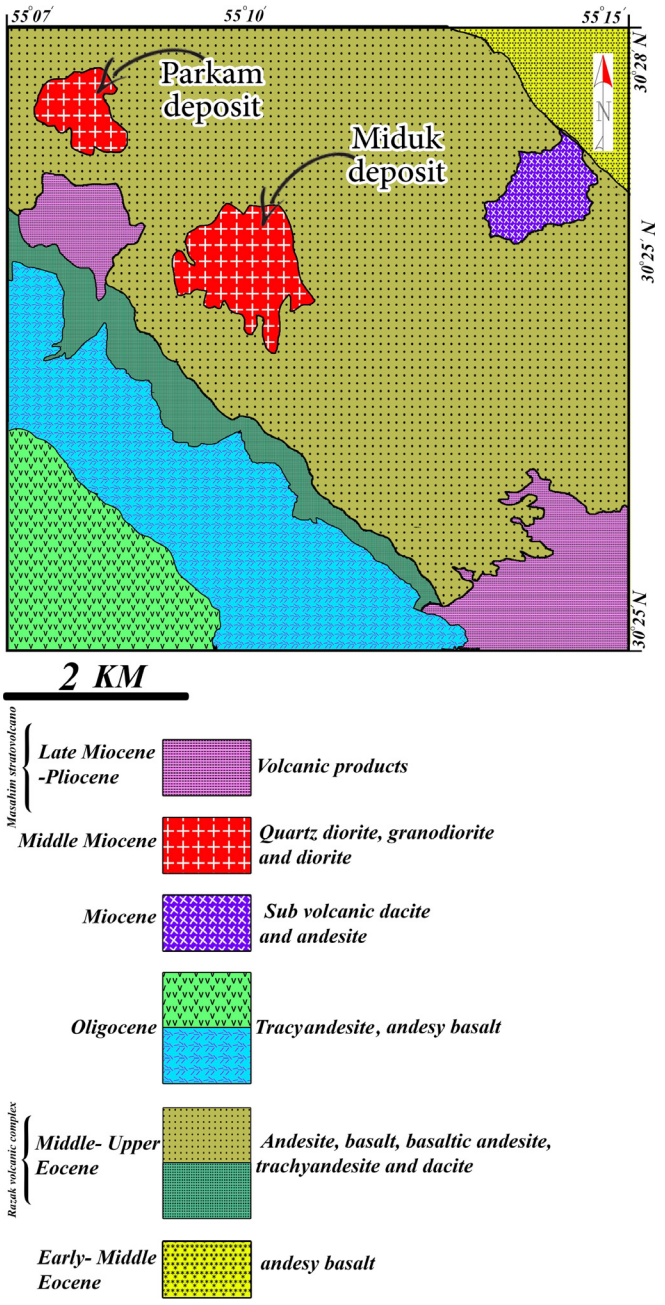

Fig. 2. Regional geological map of the Meiduk and Parkam areas, based on the geological map of Shahr-e-Babak (Modified after Saric et al., 1971).

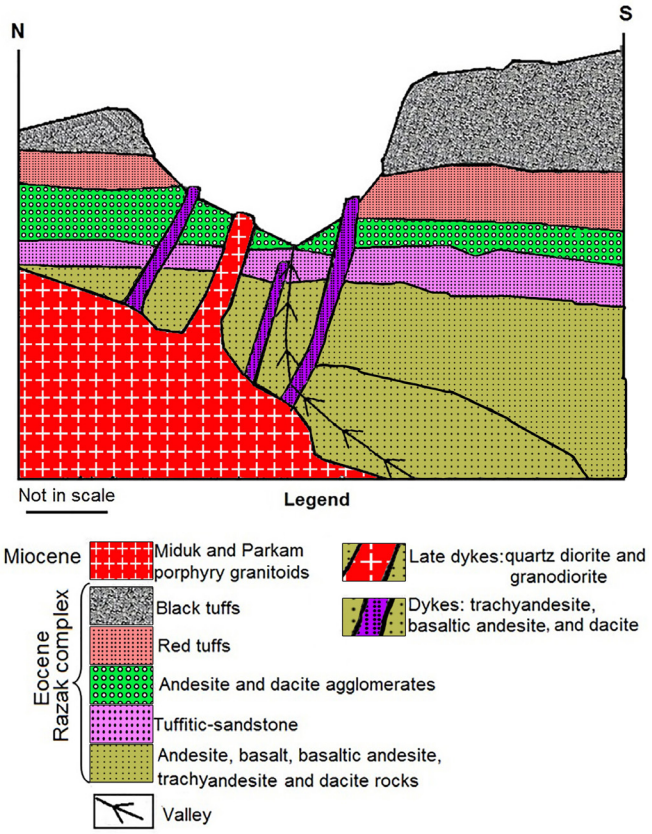

Fig. 3. Schematic cross section of MPGS and peripheral Razak complex.

Parkam porphyry granite stocks (MPGS) (Fig. 2) intruded andesite, basalt, basaltic andesite, trachyandesite and dacite of the Eocene Razak complex (Fig. 3). On the basis of the 40Ar/39Ar and U/Pb isotope age datings, Hassanzadeh (1993) and McInnes et al. (2003) reported two different ages of 11.3 ± 0.5 and 12.5 ± 0.1 Ma, respectively, for the Meiduk porphyry granitoid stocks.

Two sets of NE-SW and N-S trending dykes are exposed in the study area. The NE-SW trending dykes consist mainly of trachyandesite, basaltic andesite, and dacite porphyry rocks, intersected the pyroclastic and host volcanic rocks. While, the N-S trending dykes are mostly composed of late quartz diorite and granodiorite with weak mineralization that intersected both the Middle Miocene porphyry granitic stocks (MPGS) Meiduk and their host volcanic rocks in the Meiduk and Parkam areas (Fig. 3).

3. Analytical techniques

A total of 120 samples were collected from outcrops and drill cores from MPGS. Base on detail petrographic studies twenty eight samples ranging from fresh to least altered rocks were selected for whole rock geochemical analysis. The analyses were carried out in the Activation Laboratories Ltds (Actlabs) in Ontario, Canada. The results are given in Table 1.

Samples were digested with aqua regia and diluted to 250 ml volume. Appropriate international reference materials for the metals of interest were digested at the same time. The samples and standards were analyzed on Thermo ICAP 6500 ICP. Trace and rare earth elements concentration were analyzed by solution ICP-MS (Induced Coupled Plasma-Mass Spectrometry) at the same laboratory with method 4 Litho research (Lithium Metaborate/Tetraborate Fusion – ICP/OES and ICP/MS).

4. Petrography

Field and petrographic observations reveal that the MPGS main mineralization phases are hosted by quartz diorite, granodiorite and diorite with porphyritic and occasionally inequigranular textures. Their modal mineralogy consists of 50% plagioclase, less than 5 to 28% quartz, 4 to 17% K-feldspar, 10% biotite and 5% hornblende. Plagioclase occurs both as subhedral to euhedral phenocrysts (0.5 to 6 mm in size) and microlitic grains. They are often associated with K-feldspar, sericite, chlorite and epidote (Fig. 4a and b). K-feldspar (0.5 to 2 mm in size) is closely associated to sericite and clay minerals (Figs. 4g and h). Hornblendes (up to 6 mm in size) are pseudomorphically replaced by a mixture of biotite, magnetite and chlorite (Fig. 4c, d, I and j). Biotite occurs both as primary magmatic form and product of hydrothermal alteration. Magmatic biotites (up to 3 mm in size) are characterized by euhedral phenocrysts with distinct cleavages and dark brown to pale yellowish brown colour (Fig. 4c, d, e, f, g and h). In some thin sections magmatic biotite around the margin is slightly altered to chlorite and replaced in the core by K-feldspar and magnetite. Secondary hydrothermal biotite, formed after alteration of magmatic biotite or hornblende, is light brown in colour and occurs as flaky aggregates (Fig. 4d).

Apatite, zircon, magnetite, rutile and titanite are common accessory minerals that often occur as inclusions in plagioclase and biotite phenocrysts. The groundmass of MPGS consists mainly of fine-grained quartz, biotite, plagioclase and K-feldspar (Fig. 4).

The MPGS have been subjected to extensive potassic, phyllic and argillic alteration, enveloped by propylitic alteration halo. The potassic alteration is characterized by secondary K-feldspar in the plagioclase rims and in the matrix, as well as secondary biotite that completely replaces ferromagnesian minerals such as primary biotite and hornblende. In potassic alteration zone, barren quartz veins cut through the plagioclase phenocrysts and primary biotites. Chalcopyrite is the main Cu mineral and occurs as dissemination, intergrowth with magnetite and vein/veinlets with quartz-magnetite. In the phyllic alteration zone, characterized by the presence of quartz, sericite and pyrite, almost all of the rock-forming minerals are completely altered to sericite and pyrite. Pyrite is the most important mineral that occurs both as the veins/veinlets and as dissemination in the phyllic alteration zone. In argillic alteration zone all rock-forming minerals are completely altered to clay minerals, sericite, quartz and hematite. Propylitic zone is characterized by mafic minerals that are altered to chlorite, epidote and calcite. Also, plagioclase phenocrysts are altered to sericite, chlorite and epidote. These hydrothermal alterations are a complex series of processes involving mineralogical, chemical and textural changes as a result of hot aqueous fluids-rock interaction under evolving physico-chemical and pressure-temperature conditions (Pirajno, 2009).

5. Whole-rock geochemistry

The results of whole rock geochemical analyses of MPGS are presented in Table 1. Using petrography, alteration zones and LOI content, the rocks were divided into weak, medium and strong alteration types.

The LOI (1.36–7.29 wt%) shows that all samples were more or less affected by hydrothermal alteration. The mobility of some major and trace elements versus LOI wt% in hydrothermal alteration zones in the porphyry copper deposits are well established (Hikov, 2013), especially in re-distribution/mobilization of the alkali elements (e.g. K and Na) and strontium. Therefore, we used mainly immobile elements for classification of MPGS.

Table 1
Whole rock analyses of the Miduk and Parkam granitoid.

Analyte Symbol	MD13-389	MD11-538.2	MD11-621	MD17-187	MD11-700	MD16-428	MD12-265.2	MD13-580	MD13-687	MD11-1038	MD12-557	MD11-474.4	MD12-657.6	MD12-208.3	MD11-536.4	MD16-165	MD16-311.20	MD16-532.5	MD13-230	MD16-715.91	MD11-856.40	MD11-307.9
Rock Types	Q-DIORITE	QDIORITE	QDIORITE	G-DIORITE	G-DIORITE	QDIORITE	QDIORITE	QDIORITE	QDIORITE	QDIORITE	G-DIORITE	QDIORITE	QDIORITE	QDIORITE	QDIORITE	G-DIORITE	QDIORITE	G-DIORITE	QDIORITE	G-DIORITE	QDIORITE	QDIORITE
Locality	Meiduk	Meiduk	Meiduk	Meiduk	Meiduk	Meiduk	Meiduk	Meiduk	Meiduk	Meiduk	Meiduk	Meiduk	Meiduk	Meiduk	Meiduk	Meiduk	Meiduk	Meiduk	Meiduk	Meiduk	Meiduk	Meiduk
Type of alteration	Potassic	Potassic	Potassic	Potassic	Potassic	Phylic	Phylic	Potassic	Potassic	Potassic	Philic	Phylic	Potassic	Potassic	Phylic	Potassic	Potassic	Potassic	Phylic	Potassic	Phylic	Potassic
Alteration degree	Strong	Strong	Moderate	Minor	Moderate	Strong	Strong	Moderate	Moderate	Minor	Moderate	Moderate	Moderate	Strong	Strong	Minor	Strong	Moderate	Strong	Strong	Moderate	Strong
Source	This study	This study	This study	This study	This study	This study	This study	This study	This study	This study	This study	This study	This study	This study	This study	This study	This study	This study	This study	This study	This study	This study
SiO_2 (Wt%)	57.37	63.86	64.39	67.26	61.37	60.47	61.45	62.6	69.13	66.34	62.02	65.97	63.97	61.52	61.99	64.52	62.11	62.06	57.89	61.69	65.71	63.84
Al_2O_3	15.34	14.65	14.33	14.53	15.6	13.4	14.91	14.39	13.51	14.17	16.11	13.26	15.76	14.87	15.98	13.99	14.96	14.59	15.02	14.93	12.98	13.4
Fe_2O_3	2.42	2.09	2.87	2.93	4.25	4.62	1.52	2.94	2.52	2.44	3.03	2.3	1.65	1.58	3.09	5.27	3.43	3.21	3.2	2.33	2.53	4.5
MnO	0.02	0.01	0.01	0.03	0.018	0.01	0.01	0.01	0.01	0.01	0.02	0.01	0.01	0.01	0.02	0.02	0.02	0.01	0.01	0.03	0.01	0.01
MgO	2.08	1.52	1.52	1.71	1.65	1.83	1.49	1.7	1.34	1.37	1.73	1.32	1.93	1.56	1.72	2.27	1.37	1.75	1.97	2.09	1.54	1.36
CaO	4.52	3.93	3.81	0.43	4.43	3.96	3.47	3.94	0.96	2.15	3.61	3.47	3.27	4.02	4.61	0.39	3.6	4.21	4.28	4.05	2.99	3.83
Na_2O	3.45	4.01	3.72	2.78	4.57	3.47	6.45	4.42	2.3	3.27	4.61	4.51	4.62	3.76	5.01	2.74	4.92	3.74	5.04	5.28	3.08	3.7
K_2O	4.08	3.92	4.33	6.25	2.38	4.15	1.24	3.16	5.7	5.52	2.9	2.69	3.6	3.6	2.17	6.16	2.84	4.17	2.6	2.39	4.6	3.67
TiO_2	0.65	0.447	0.48	0.43	0.57	0.53	0.51	0.49	0.38	0.45	0.49	0.42	0.54	0.52	0.52	0.46	0.44	0.49	0.58	0.55	0.45	0.44
P_2O_5	0.25	0.15	0.18	0.16	0.3	0.22	0.27	0.21	0.17	0.2	0.21	0.08	0.2	0.26	0.24	0.06	0.18	0.22	0.22	0.2	0.2	0.19
LOI	8.34	5.47	4.67	2.33	4.33	5.66	7.29	5.03	3.21	2.93	5.13	4.83	5.2	6.58	5.16	2.6	5.85	5.05	7.17	5.39	4.02	5.4
Total	98.53	100.1	100.3	98.85	99.48	98.35	98.62	98.9	99.25	98.86	99.87	98.87	100.8	98.3	100.5	98.48	99.74	99.53	97.99	98.94	98.11	100.3
Sc (ppm)	7	5	6	5	7	7	5	6	4	5	7	5	7	6	7	6	5	6	7	7	6	5
Be	2	1	1	1	2	1	1	2	1	1	2	1	2	2	2	1	1	1	2	2	1	1
V	94	69	76	75	88	93	62	79	62	58	82	59	95	82	75	85	68	76	79	88	68	69
Ba	438	441	460	399	548	407	162	459	435	658	517	306	526	535	497	496	558	637	290	252	545	484
Sr	616	649	657	271	803	539	395	694	259	477	754	558	669	609	825	275	697	707	637	607	534	671
Y	10	9	8	6	12	11	11	10	6	7	11	7	8	8	10	5	8	8	12	9	7	9
Zr	130	114	125	106	143	110	126	118	97	124	128	114	135	132	123	115	122	129	118	126	108	105
Cr	80	90	50	130	60	40	40	50	80	50	70	60	50	50	70	50	60	70	50	50	110	60
Co	3	3	5	4	6	7	3	5	3	5	20	3	3	2	16	20	4	8	5	5	3	6
Ni	20	20	20	20	20	20	20	20	20	20	20	20	20	20	20	20	20	20	20	20	20	20
Cu	5190	4620	5960	4060	2980	6590	1280	6190	6100	7060	1620	5150	3370	4100	2500	4790	3650	4420	2820	2950	7630	5220
Zn	40	<30	<30	80	<30	50	90	<30	<30	<30	40	<30	50	<30	50	50	40	30	40	30	<30	30
Ga	16	17	17	15	20	18	14	17	13	17	18	17	16	16	20	18	20	18	17	16	16	17
Ge	2	2	2	3	2	2	2	2	3	2	2	2	2	2	2	2	2	1	2	2	1	2
As	<5	<5	<5	751	<5	<5	<5	<5	301	<5	<5	<5	6	<5	<5	<5	6	<5	<5	<5	<5	<5
Rb	91	65	69	127	52	80	52	69	113	95	62	55	86	75	44	112	55	69	80	80	78	62
Nb	9	7	7	6	10	6	7	7	5	7	7	8	9	8	7	6	6	8	8	7	6	5
Mo	25	48	9	7	<2	3	24	24	26	3	12	<2	27	49	6	4	6	3	8	14	<<2	7
Ag	1	0.8	1.3	0.9	1.1	0.8	5.5	1.1	0.8	1.5	1	1	1.2	1.1	0.9	0.6	23.4	0.7	2.2	1.7	1.5	1.2
Sn	5	2	2	2	<1	2	3	2	3	<1	3	2	3	4	1	2	2	2	2	<1	1	2
Sb	<0.50	<0.50	1.2	5.2	<0.50	<0.50	2	<0.50	2.4	<0.50	<0.50	<0.50	<0.50	<0.50	<0.50	<0.50	8.9	<0.50	<0.50	<0.50	<0.5	<0.50
Cs	2.4	1.3	<0.50	3.7	1.4	1.3	0.7	1.3	3	0.8	1.2	0.7	3.9	2.4	0.9	1.2	1.7	0.9	1.5	2.3	0.7	1.1
La	31.1	26.4	26.8	26.4	34.9	27.4	31.9	34.8	28.1	14.3	34.7	26	33.9	32.8	29.7	12.8	23	29.3	33.4	29.9	20.4	24.1
Ce	55.5	46.8	47.3	44.1	64.4	50.8	56.4	59.3	48.1	27	58.8	44.5	57.9	56.7	54.5	22.7	41.8	53.4	58.8	52	37.1	44.5
Pr	6.05	5.01	4.95	4.63	7	5.65	6.01	6.18	4.88	3.09	6.15	4.67	6.11	6.02	6.16	2.57	4.73	5.85	6.39	5.64	4.14	4.95
Nd	22.9	19.1	18.1	16.3	25.9	22.4	22.6	22.3	17.7	11.9	22.6	17.4	22.2	22.4	23.3	9.6	18.2	22.9	23.7	21	15.9	18.7
Sm	4.1	3.3	2.9	2.5	4.5	3.8	4	3.7	2.7	2.4	3.7	2.9	3.5	3.6	4.1	1.7	3.1	4.1	3.9	3.5	2.9	3.4
Eu	1.1	0.91	0.8	0.63	1.09	0.89	1.07	1	0.7	0.63	0.96	0.76	0.92	1.03	1.12	0.55	0.82	0.99	1.12	1	0.63	0.78
Gd	2.7	2.3	1.9	1.6	3	2.6	2.5	2.5	1.7	1.6	2.4	1.8	2.3	2.4	2.6	1.3	2.2	2.4	2.7	2.2	2	2.2
Tb	0.4	0.3	0.3	0.2	0.4	0.4	0.4	0.3	0.2	0.2	0.3	0.2	0.3	0.3	0.4	0.2	0.3	0.3	0.4	0.3	0.3	0.3
Dy	1.9	1.5	1.3	1	2.1	1.9	1.8	1.7	1.1	1.1	1.6	1.1	1.5	1.6	1.9	0.8	1.5	1.8	1.8	1.6	1.3	1.5
Ho	0.3	0.3	0.3	0.2	0.4	0.3	0.3	0.3	0.2	0.2	0.3	0.2	0.3	0.3	0.3	0.2	0.3	0.3	0.3	0.3	0.2	0.3
Er	0.9	0.7	0.7	0.5	0.9	0.9	0.9	0.9	0.5	0.6	0.8	0.6	0.7	0.8	0.9	0.5	0.8	0.9	0.9	0.8	0.7	0.7
Tm	0.14	0.1	0.09	0.07	0.12	0.14	0.12	0.13	0.08	0.09	0.11	0.08	0.1	0.11	0.13	0.07	0.11	0.13	0.13	0.12	0.1	0.1
Yb	0.9	0.6	0.6	0.5	0.8	0.8	0.8	0.9	0.5	0.5	0.7	0.5	0.7	0.7	0.8	0.4	0.6	0.8	0.8	0.7	0.6	0.7
Lu	0.13	0.1	0.08	0.08	0.13	0.12	0.11	0.12	0.08	0.08	0.12	0.08	0.1	0.11	0.12	0.06	0.1	0.12	0.12	0.1	0.1	0.1
Hf	2.8	2.5	2.6	2.5	3.2	2.3	3.1	2.7	2	2.8	2.9	2.7	3.2	3.1	2.7	2.6	2.4	3	2.9	2.8	2.1	2
Ta	0.7	0.6	0.6	0.6	0.8	0.6	0.7	0.6	0.5	0.6	0.6	0.6	0.7	0.7	0.6	0.6	0.6	0.6	0.6	0.6	0.6	0.5
W	9	2	2	6	2	1	12	7	6	1	7	1	12	11	1	3	2	2	6	4	2	2
Tl	0.8	0.5	0.5	1.5	0.4	0.5	0.4	0.5	1	0.5	0.5	0.4	0.6	0.6	0.3	0.7	0.5	0.5	0.6	0.5	0.5	0.6
Pb	13	12	19	16	11	13	23	13	9	16	15	12	19	22	15	10	43	17	15	16	9	18
Bi	<0.40	0.5	<0.40	<0.40	1.1	<0.40	<0.40	<0.40	<0.40	1.3	<0.40	<0.40	<0.40	<0.40	<0.40	<0.40	<0.40	<0.40	<0.40	<0.40	1.4	<0.4
Th	7.3	9.8	10.4	7.7	12.5	10.3	10.3	10.2	7.2	9.8	10.2	9.7	10.8	10.3	11.9	8.9	10.7	11.1	9.9	7.1	9.8	9.7
U	2.5	1.2	1.1	1.3	1.5	1.9	3.4	2.1	1.2	1.1	3.2	1.2	3.4	3.3	2.9	0.8	1.7	1.9	2.7	1.7	1	1.8
Mg#	46.22	42.1	34.62	36.85	27.96	28.37	49.5	36.63	34.71	35.95	36.34	36.46	53.91	49.68	35.75	30.1	28.54	35.28	38.1	47.28	37.83	23.2
Th/Yb	8.11	16.33	17.33	15.4	15.62	12.87	12.87	11.33	14.4	19.6	14.57	19.4	15.42	14.71	14.8	22.25	17.83	13.87	12.37	10.14	16.33	13.85
La/Yb	34.55	44	44.66	52.8	43.62	34.25	39.87	38.66	56.2	28.6	49.57	52	48.42	46.85	37.12	32	38.33	36.62	41.75	42.71	34	34.42
LaN/YbN	24.78	31.56	32.03	37.87	31.29	24.56	28.6	27.73	40.31	20.51	35.55	37.29	34.73	33.61	26.62	22.95	27.49	26.27	29.94	30.63	24.38	24.69
Rb/Sr	0.14	0.1	0.1	0.46	0.06	0.14	0.13	0.09	0.43	0.19	0.08	0.09	0.12	0.12	0.05	0.4	0.07	0.09	0.12	0.13	0.14	0.09

(*continued on next page*)

Table 1 (*continued*)

Analyte Symbol	MD13-389	MD11-538.2	MD11-621	MD17-187	MD11-700	MD16-428	MD12-265.2	MD13-580	MD13-687	MD11-1038	MD12-557	MD11-474.4	MD12-657.6	MD12-208.3	MD11-536.4	MD16-165	MD16-311.20	MD16-532.5	MD13-230	MD16-715.91	MD11-856.40	MD11-307.9
K_2O/Na_2O	1.18	0.98	1.16	2.25	0.52	1.20	0.19	0.71	2.48	1.69	0.63	0.60	0.78	0.96	0.43	2.25	0.58	1.11	0.52	0.45	1.49	0.99
Dy/Yb	2.11	2.50	2.17	2.00	2.63	2.38	2.25	1.89	2.20	2.20	2.29	2.20	2.14	2.29	2.38	2.00	2.50	2.25	2.25	2.29	2.17	2.14
La/Yb	34.56	44.00	44.67	52.80	43.63	34.25	39.88	38.67	56.20	28.60	49.57	52.00	48.43	46.86	37.13	32.00	38.33	36.63	41.75	42.71	34.00	34.43
Sr/Y	61.60	72.11	82.13	45.17	66.92	49.00	35.91	69.40	43.17	68.14	68.55	79.71	83.63	76.13	82.50	55.00	87.13	88.38	53.08	67.44	76.29	74.56
Eu/Eu^*	1.01	1.01	1.04	0.96	0.91	0.87	1.03	1.01	1.00	0.98	0.98	1.02	0.99	1.07	1.05	1.13	0.96	0.96	1.06	1.10	0.80	0.87

PM28-173.1	PM6-242.3	PM6-184.8	PM14-201	PM26-110.4	PM17-17	p-2	p-8	p-15	p-13	p-1	p-3	p-4	p-5
QDIORITE	QDIORITE	QDIORITE	G-DIORITE	QDIORITE	G-DIORITE	DIORITE	DIORITE	DIORITE	DIORITE	Q-DIORITE	Q-DIORITE	Q-DIORITE	Q-DIORITE
Parkam	Parkam	Parkam	Parkam	Parkam	Parkam	Parkam	Parkam	Parkam	Parkam	Parkam	Parkam	Parkam	Parkam
Fresh	Potassic	Phylic	Potassic	Phylic	Fresh	Potassic	Potassic	Fresh	Fresh	Fresh	Fresh	Potassic	Fresh
Minor	Moderate	Moderate	Moderate	Minor	Minor	Strong	Strong	Minor	Minor	Minor	Minor	Moderate	Minor
This study	This study	This study	This study	This study	This study	Mohamadi Laghab., 2011	Mohamadi Laghab., 2011	Mohamadi Laghab., 2011	Mohamadi Laghab., 2011	Mohamadi Laghab., 2011	Mohamadi Laghab., 2011	Mohamadi Laghab., 2011	Mohamadi Laghab., 2011
63.46	62.59	61.2	61.06	61.32	61.03	59.6	59.4	61.8	60.7	62.4	61.8	60.5	60.4
17.05	16.8	16.36	16.85	16.44	16.92	16.7	16.25	16.75	16.55	16.7	16.65	16.2	16.4
5.66	5.16	4.96	5.77	4.74	5.69	4.31	5.65	5.35	4.8	4.33	5.13	3.13	4.42
0.03	0.02	0.1	0.06	0.08	0.081	0.08	0.21	0.05	0.05	0.04	0.08	0.02	0.07
2.17	2.34	2.23	2.35	2.01	2.55	2.09	2.34	2.51	2.14	2.29	2.18	1.98	2.24
2.43	2.42	4.58	4.18	4.22	3.32	4.82	3.63	4.16	4.75	3.75	4.09	4.94	5.03
3.75	2.86	4.03	3.25	4.34	4.08	4	3.19	4.04	4.24	3.69	4.44	3.43	4.51
2.27	3.72	2.69	3.13	2.81	2.54	3.03	2.78	2.54	2.91	2.7	2.26	3.77	2.74
0.5	0.5	0.52	0.56	0.51	0.62	0.52	0.54	0.56	0.53	0.52	0.54	0.49	0.53
0.23	0.22	0.22	0.22	0.2	0.21	0.21	0.24	0.22	0.22	0.22	0.22	0.21	0.21
2.57	3.55	3.87	3.33	2.94	2.83	4.2	4.77	1.36	2.38	2.11	2.08	3.18	1.49
100.1	100.2	100.8	100.8	99.63	99.88	99.7	99.1	99.5	99.5	98.7	99.7	98.1	98.2
8	9	9	9	8	10								
103	102	106	108	105	127	89	93	106	92	92	89	87	89
655	940	927	1017	884	781	814	348	716	904	718	786	776	821
774	679	926	858	919	903	748	199.5	870	958	795	860	990	836
10	10	10	9	9	12	9	9	10	9	9	10	8	9
117	114	101	116	105	102	93	103	109	108	114	116	100	94
60	120	40	80	40	40	10	20	20	20	20	20	20	20
9	10	12	16	13	15	10	8.8	12.8	11.5	7.8	11.7	12.3	11.2
20	20	20	20	20	20								
240	470	50	50	90	130	11	136	374	9	215	18	1650	26
40	<30	80	60	80	580	64	135	37	42	21	62	19	54
20	21	19	20	21	21	19	19	20	20	19	20	17	19
1	2	2	2	1	2								
<5	<5	<5	<5	<5	<5								
61	100	65	55	75	69	81	82	62	70	65	56	86	74
5	4	4	5	5	4	4	5	6	6	6	5	6	5
<2	<2	3	2	3	<2								
0.8	0.9	0.6	1	0.8	0.9								
2.6	2.2	1.5	0.6	3.2	4.5	4.17	3.4	1.89	0.68	1.89	1.47	2.8	0.76
32.2	32.3	27.9	27.5	27.2	27.8	25	26.5	29.9	29.5	30.7	28.6	28.4	25.4
53.9	54.8	47.8	47.5	46.4	48.4	48.2	49.4	58.3	56.3	57.9	55.1	53	48.8
5.62	5.77	5.14	5.13	5.08	5.38								
21.2	20.8	19.5	19.4	19.7	21.1	17.3	16.7	19.9	19.5	19.6	19.6	17.7	17.5
3.6	3.6	3.4	3.5	3.3	3.9	3.06	2.91	3.46	3.31	3.35	3.44	2.79	3.1
0.95	0.99	0.98	0.91	0.95	1.06	1	0.97	1.14	1.11	1.1	1.15	0.98	1.07
2.5	2.4	2.3	2.5	2.3	2.8	3.08	3.13	3.72	3.42	3.38	3.51	3.06	3.26
0.3	0.3	0.3	0.3	0.3	0.4	0.38	0.4	–	–	–	–	–	–
1.6	1.7	1.7	1.6	1.7	2	1.7	1.9	2.1	1.9	1.86	2.06	1.64	1.86
0.3	0.3	0.3	0.3	0.3	0.4								
0.9	0.8	0.9	0.9	0.9	1	1	1	1.14	1.01	1.01	1.07	0.91	1.06
0.13	0.12	0.14	0.13	0.13	0.16	0.11	0.11	0.14	0.12	0.11	0.14	0.12	0.11
0.8	0.8	0.9	0.8	0.8	0.9	0.8	0.8	0.95	0.94	0.89	0.94	0.76	0.9
0.12	0.12	0.13	0.12	0.11	0.13								
2.6	2.5	2.3	2.6	2.4	2.4	2.7	2.9	3.1	3.1	3.2	3.3	2.8	2.8
0.5	0.7	0.4	0.5	0.5	0.4	0.4	0.4	0.5	0.5	0.5	0.5	0.5	0.4
<1	5	<1	2	<1	1	1	3	1	1	2	1	3	1
0.4	0.5	0.4	0.2	0.4	0.4								
7	<5	9	11	10	10	7	26	6	9	7	15	8	6
16.7	14.7	12.5	13.7	11.8	11.4	12.6	12.65	15.75	15.85	17.25	13.4	14.9	12.15
5.3	4.4	4.6	4.9	4.5	3.9	3.9	3.16	4.22	4.99	5.17	4.06	3.67	3.72
27.71	31.2	31.01	28.94	29.77	30.94	32.65	29.28	31.93	30.83	34.59	29.82	38.74	33.63
20.87	18.37	13.88	17.12	14.75	12.66	15.75	15.8125	16.57	16.86	19.38	14.25	19.6	13.5

Table 1 (*continued*)

PM28-173.1	PM6-242.3	PM6-184.8	PM14-201	PM26-110.4	PM17-17	p-2	p-8	p-15	p-13	p-1	p-3	p-4	p-5
40.25	40.37	31	34.37	34	30.88	31.25	33.12	31.47	31.38	34.49	30.42	37.36	28.22
28.87	28.96	22.23	24.65	24.38	22.15	22.41	23.76	22.57	22.51	24.74	21.82	26.8	20.24
0.07	0.14	0.07	0.06	0.08	0.07	0.1	0.41	0.07	0.07	0.08	0.06	0.08	0.08
0.61	1.30	0.67	0.96	0.65	0.62	0.76	0.87	0.63	0.69	0.73	0.51	1.10	0.61
2.00	2.13	1.89	2.00	2.13	2.22	2.13	2.38	2.21	2.02	2.09	2.19	2.16	2.07
40.25	40.38	31.00	34.38	34.00	30.89	31.25	33.13	31.47	31.38	34.49	30.43	37.37	28.22
77.40	67.90	92.60	95.33	102.11	75.25	83.11	22.17	87.00	106.44	88.33	86.00	123.75	92.89
0.97	1.03	1.07	0.94	1.05	0.98	1.00	0.98	0.97	1.01	1.00	1.01	1.03	1.03

The SiO_2 content of Meiduk and Parkam studied rocks range from 57.89 to 69.13% and 59.4 to 63.46%, respectively. In the total alkali silica diagram (Cox et al., 1979) the Meiduk samples plot mainly in the fields of granodiorite and granite, whereas Parkam samples fall within the field of granodiorite or close to the diorite-granodiorite boundary (Fig. 5a).

In the SiO_2 versus Zr/TiO_2 diagram, the MPGS are mainly placed in the fields of rhyodacite, dacite and andesite that are volcanic equivalent of granodiorite, quartzdiorite and diorite, respectively (Fig. 5b). All these rock samples are sub-alkaline in origin (Figs.5a and 11a). As shown in the K_2O versus SiO_2 diagram, the Parkam samples fall within the field of high-K calc-alkaline, whereas the Meiduk rocks are placed in the fields of high-K calc-alkaline and shoshonite (Fig. 6). On the Th/Yb versus Ta/Yb diagram, the MPGS fall in the shoshonite field (Fig. 10b). Using Y versus Zr diagram the MPGS are placed in the field of calc-alkaline magmatic series (Fig. 7) that show high oxygen fugacity during crystallization. Using A/CNK versus A/NK diagram of Maniar and Piccoli (1989) the MPGS are plotted mainly in the field of metaluminous to weakly peraluminous (Fig. 8) that can be attributed either to the differentiation of hornblende or water content in the melting zone (Zen, 1986; Waight et al., 1998). However, the mineralogy of the MPGS, that include biotite, hornblende, magnetite, apatite and zircon, absence of Al rich mineral such as cordierite, corundum, topaz as well as lack of crustal enclaves points to their metaluminous nature. The SiO_2 content, molecular A/CNK ratio, K_2O/Na_2O ratio, main modal minerals (such as hornblende and biotite), and chemical composition of MPGS all confirm their I-type characteristics (Harris et al., 1986).

6. Tectonic setting

Based on the Ta versus Yb and Nb versus Y discrimination diagrams of Pearce et al. (1984), the MPGS are plotted in the field of volcanic arc granite (VAG) in the collisional tectonic setting (Fig. 9). The VAG characteristics together with high ratios of La/Yb versus Th/Yb (Condie, 1989) and Th/Yb versus Ta/Yb (Pearce et al., 1990) are indications of their formation in an active continental margin environment (Fig. 10). In the tectonic setting diagrams of R_1 versus R_2 (De La Roche et al., 1980) and Th/Yb versus Th/Sm (Zhu et al., 2009 b) the MPGS are mostly plotted in the post-collisional and late orogenic fields (Fig. 11). The sub-alkaline trend of the MPGS is clear in Fig. 11a, where they plot in the high-potassic calc-alkaline and sub-alkaline monzonitic fields. Also, in Fig. 11a, only samples with shoshonitic affinity from Meiduk (see Fig. 6) are plotted in the late orogenic field that may point to a relationship between their higher amount of K_2O and an increase in crustal thickness.

7. Assessment of adakitic nature

The most important geochemical characteristics of adakites are: $SiO_2 > 56$ wt%, $Al_2O_3 > 15$ wt% (rarely lower), MgO < 3 wt%, positive Eu anomaly ($Eu/Eu^* \geq 1$), low heavy REE (HREE) contents (e.g. Y < 18 ppm, Yb < 1.8 ppm), Sr/Y > 20, high Sr content (>400 ppm), $^{87}Sr/^{86}Sr < 0.705$, high Cr (>30 ppm) and Ni (>20 ppm) contents and $(La/Yb)_N > 20$ (Defant and Drummond, 1990; Martina et al., 2005; Richards and Kerrich, 2007). The geochemical characteristics of MPGS such as their Al_2O_3 content (an average of 15.36 wt%), high Sr consent (an average of 672.73 ppm), the low Yb (an average of 0.74 ppm) and Y (an average of 9.02 ppm) contents, strongly differentiated REE patterns ($La/Yb \geq 20$) and lack of Eu anomaly ($Eu/Eu^* = 0.79–1.13$ for the Meiduk and $Eu/Eu^* = 0.96–1.07$ for the Parkam) all indicates their similarity with those of adakitic magma. Furthermore, their adakitic nature are also presented in

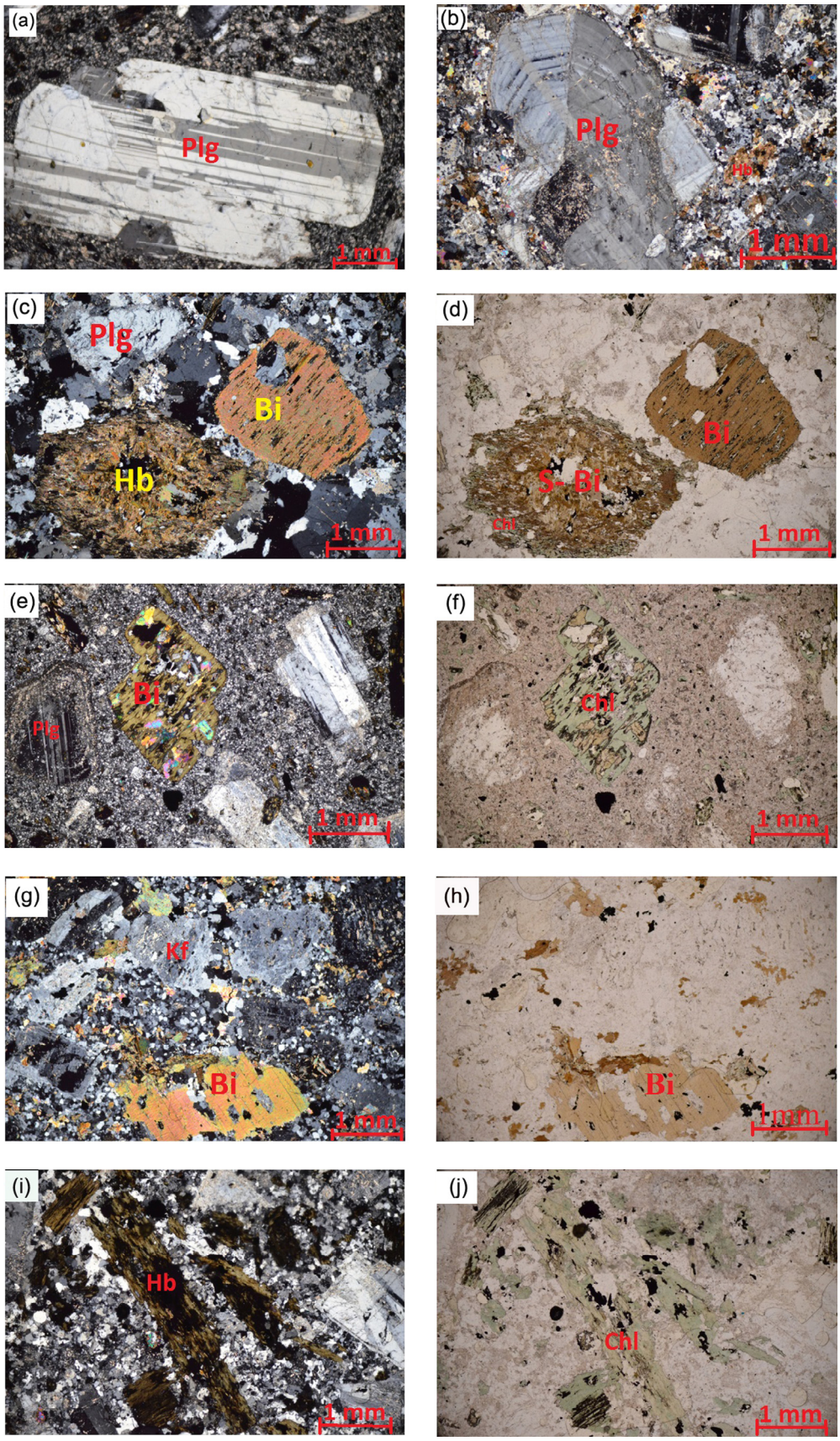

Fig. 4. photomicrographs of MPGS; (a) and (b) Plagioclase (plg) and hornblende (Hb) in quartz diorite, cross-polarized light; (c) Biotite (Bi), hornblende and plagioclase in quartz diorite; cross-polarized light; (d) Alteration of hornblende to secondary biotite (S-Bi) and chlorite (Ch) in quartz diorite; plane-polarized light; (e) and (f) Alteration of biotite to chlorite in diorite; cross-polarized light and plane-polarized light; (g) and (h) K-feldspar (Kf) and biotite in granodiorite; cross-polarized light and plane-polarized light: (I) and (j) Alteration of hornblende to chlorite in quartz diorite; cross-polarized light and plane-polarized light.

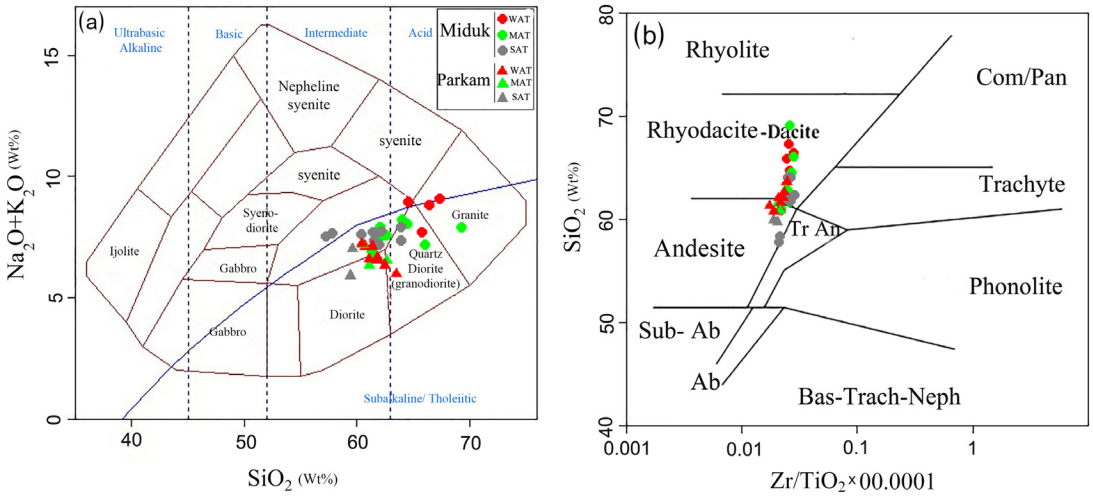

Fig. 5. (a) Total alkalis versus SiO_2 diagram for classification of the MPGS (TAS diagram after Cox et al., 1979). (b) SiO_2 versus Zr/TiO_2 diagram for classification of the MPGS (after Winchester and Floyd, 1977). WAT, weakly altered type; MAT, moderately altered type; SAT, strongly altered type.

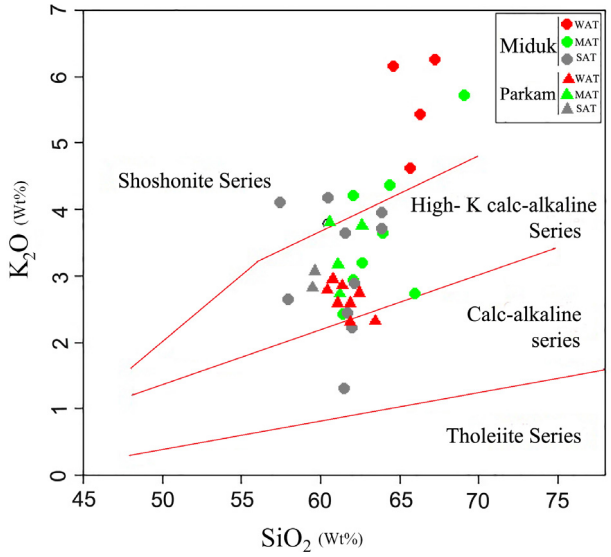

Fig. 6. K_2O versus SiO_2 diagram for MPGS (Peccerillo and Taylor, 1976).

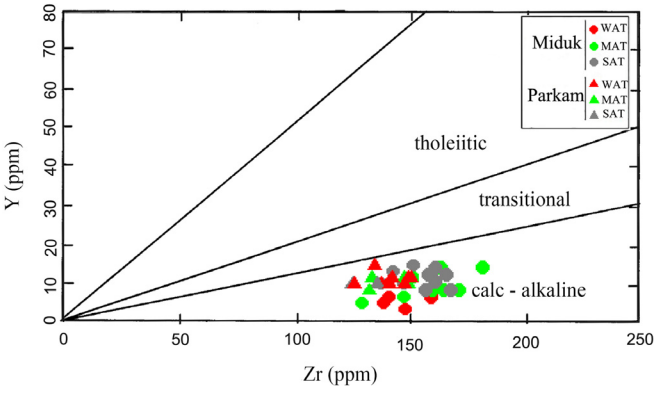

Fig. 7. Classification of the MPGS in Y versus Zr diagram (MacLean and Barrett, 1993).

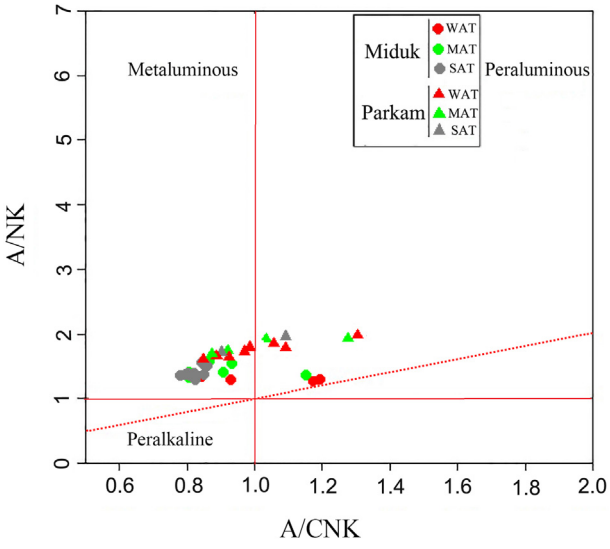

Fig. 8. Classification of the MPGS in A/NK versus A/CNK diagram [ANK = molar $Al_2O_3/(Na_2O + K_2O)$ and ACNK = molar $Al_2O_3/(CaO + Na_2O + K_2O)$, Maniar and Piccoli (1989)].

Sr/Y versus Y and La_n/Yb_n versus Yb_n discrimination diagrams (Fig. 12), where they plot in the field of adakite rather than classical arc volcanic rocks.

Primitive mantle normalized plot of trace elements (Fig. 13) show that the MPGS are depleted in HFSE (such as Ti, U, Th, Nb, Zr, P), enriched in LFSE (such as K, Rb, Cs, Sr, Pb) and have negative Nb, Ti, P anomalies. These together with enrichment in LREE relative to HREE and insignificant Eu anomalies in the chondrite-normalized REE patterns (Fig. 14) are consistent with post-collisional Miocene adakite-like rocks in the southern Tibet (Li et al., 2011; Lu et al., 2015; Yang et al., 2015). The enrichment in LFSE and conspicuous negative anomalies of Nb and Ti are typical of magmatism associated with subduction zones (Kogiso et al., 1997; Ozdemir, 2011; Imer et al., 2014). The REE pattern also indicates the formation and emplacement of MPGS in an active continental margin (Ozdemir, 2011). Lack of Eu anomaly and positive Sr anomaly (Figs. 13 and 14) show that little or no plagioclase has been segregated as cumulates or restites in the deep magma chamber before emplacement of the residual melt in the upper crust (Prouteau et al., 1999; Lu et al., 2015, 2016).

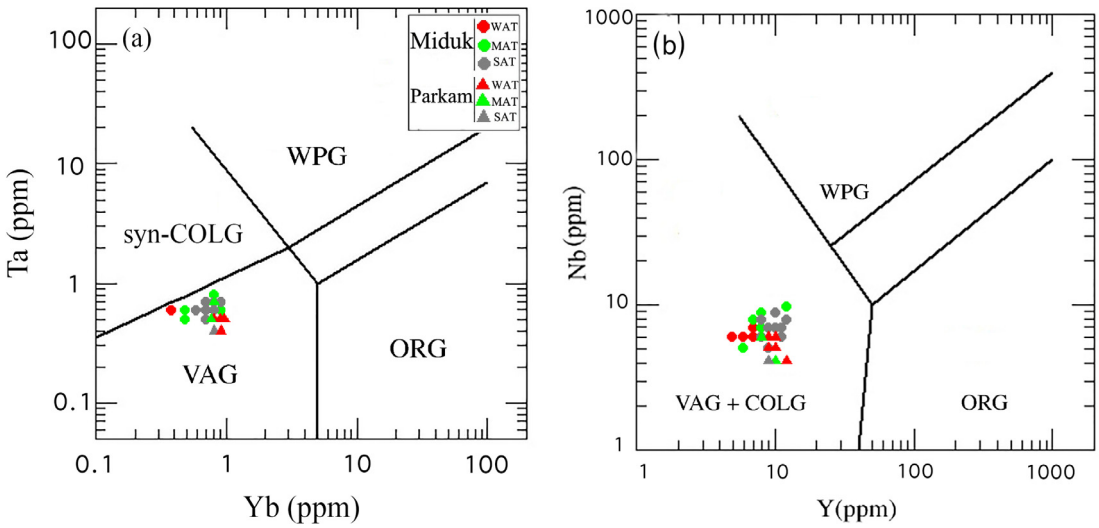

Fig. 9. Tectonic classification diagrams for the MPGS: (a) Ta versus Yb (ppm), (b) Nb (ppm) versus Y (ppm). Fields (after Pearce et al., 1984) and Pearce (1996): WPG, within plate granites; VAG, volcanic arc granites; COL, collision granites; ORG, ocean ridge granites.

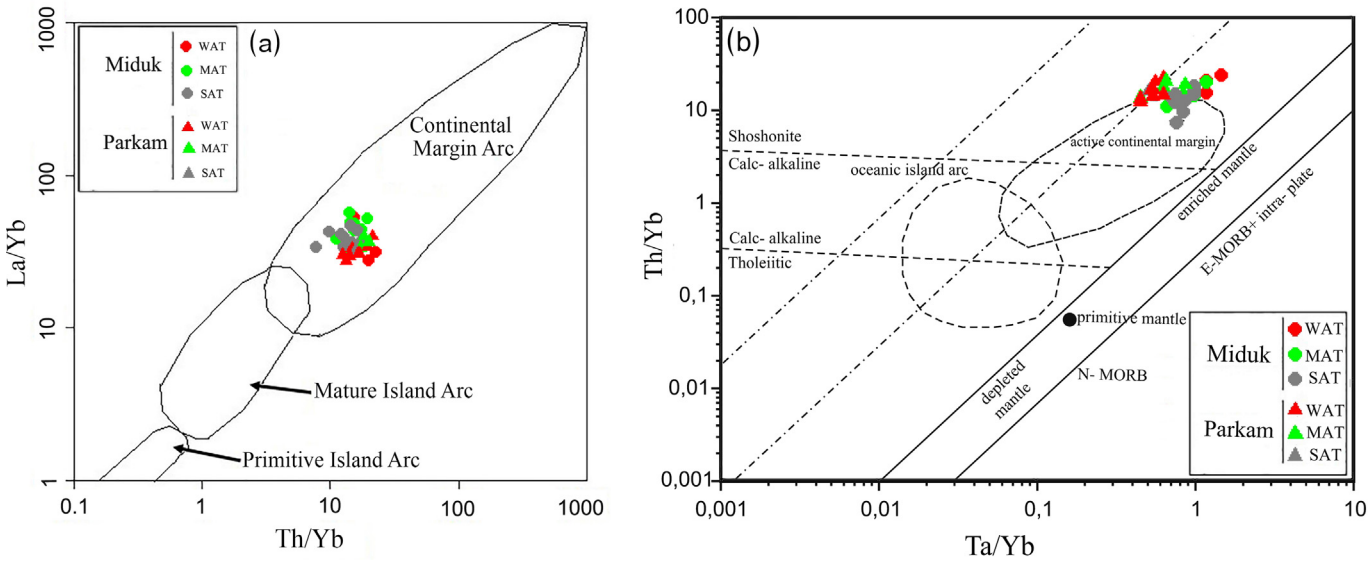

Fig. 10. Plot of MPGS on the (a) La/Yb versus Th/Yb diagram of Condie (1989) and (b) Th/Yb versus Ta/Yb discrimination diagram of Pearce et al. (1990).

The adakitic signatures not only results from oceanic slab melting but also can be caused by crustal involvement either as a source of contamination or as a protolith after crustal thickening (Petford and Atherton, 1996; Kay and Mpodozis, 2002). Hence, a combination of geochemical and geodynamic evidences should be considered for better recognition of adakitic like features of MPGS and its origin. In the subsequent section we will examine evidences for the source of the MPGS.

8. Possible sources of MPGS

Several studies indicated that in a post-collisional tectonic setting, the melting of young and hot subducted oceanic lithosphere (Martin, 1999; Kay, 1987; Defant and Drummond, 1990) or partial melting of over thickened mafic lower crust equilibrated with a garnet-hornblende residual mineralogy (Kay et al., 1987, 1991; Petford and Atherton, 1996; Kay and Mpodozis, 2001) can generate magma with adakitic signatures. In addition, the high-pressure differentiation involving amphibole and magma mixing of hydrous mafic magmas under compressive tectonic regime have been suggested for the adakite-like granitoid porphyries (Rohrlach and Loucks, 2005; Loucks, 2014; Lu et al., 2015).

It is obvious in Table 1 and Fig.15 that the high La/Yb (≥20) ratio indicates generation of MPGS parental magma at the pressure between 12 and 15 kb (crustal thickness of 40–50 km). This is in accordance with Dehghani and Makris (1983) research on the crustal thickness (45–55 km) in the study area, which was resulted due to the subduction of the Neo-Tethys oceanic lithosphere under the Central Iranian microcontinent for most of Mesozoic and Cenozoic Eras (Berberian et al., 1982; Ricou, 1994; Mohajjel et al., 2003; Alavi, 2007), that led to the collision of the Iranian and Arabian plates in the Late Eocene time (Agard et al., 2005; Allen and Armstrong, 2008; Horton et al., 2008; Hempton, 1987; Beydoun et al., 1992; Dragahi et al., 2008). The collision resulted thickening and shortening of the continental crust by folding, thrusting, and uplift of the Iranian plateau (Ricou, 1994; Mohajjel et al., 2003).

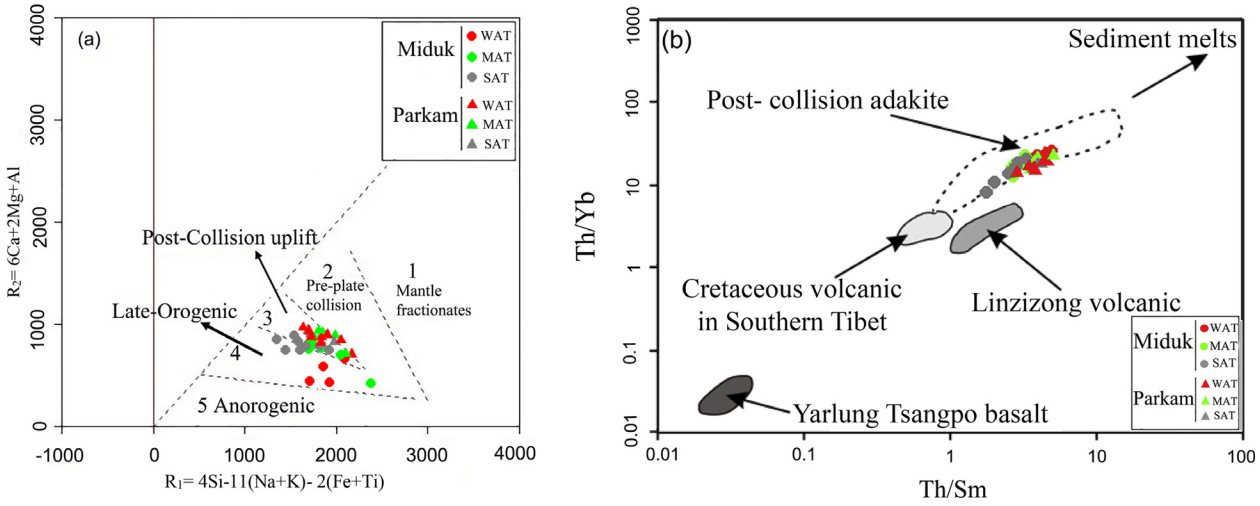

Fig. 11. Tectonic discriminant diagrams for the MPGS: (a) R1 versus R2 (after De La Roche et al., 1980) displaying the geotectonic fields (Batchelor and Bowden, 1985) as well as their petrological equivalents (Lameyre and Bowden, 1982): group 1, tholeiitic; group 2, calc-alkaline and trondhjemitic; group 3, high-potassic calc-alkaline; group 4, sub-alkaline monzonitic; group 5, alkaline and peralkaline, (b) Th/Yb versus Th/Sm (Zhu et al., 2009b).

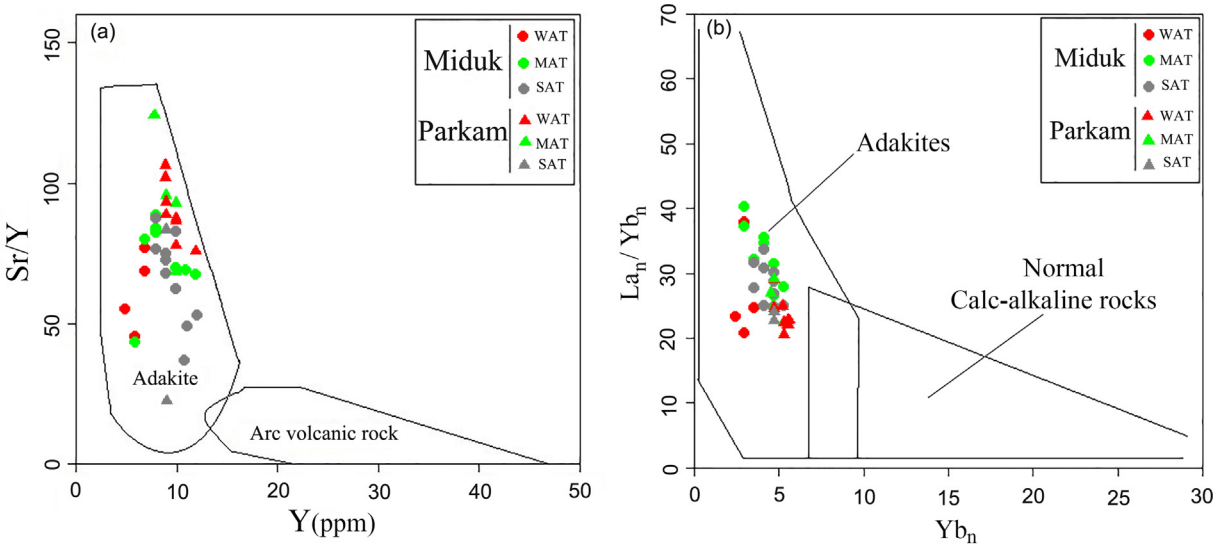

Fig. 12. Discrimination diagrams for showing the adakitic nature of MPGS: (a) Y versus Sr/Y (after Defant and Drummond, 1990), (b) Yb_N versus $(La/Yb)_N$ (after Reich et al., 2003).

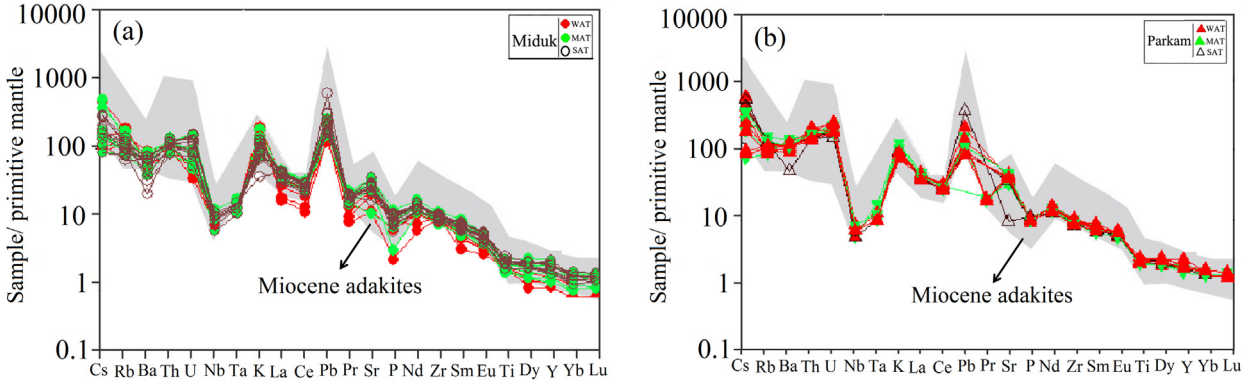

Fig. 13. Primitive mantle normalized trace element abundances for representative samples for: a- Meiduk and b- Parkam porphyry granitoids and their comparison with Miocene adakite-like high Sr/Y rocks in south Tibet (Li et al., 2011). The normalizing values are from Sun and McDonough (1989).

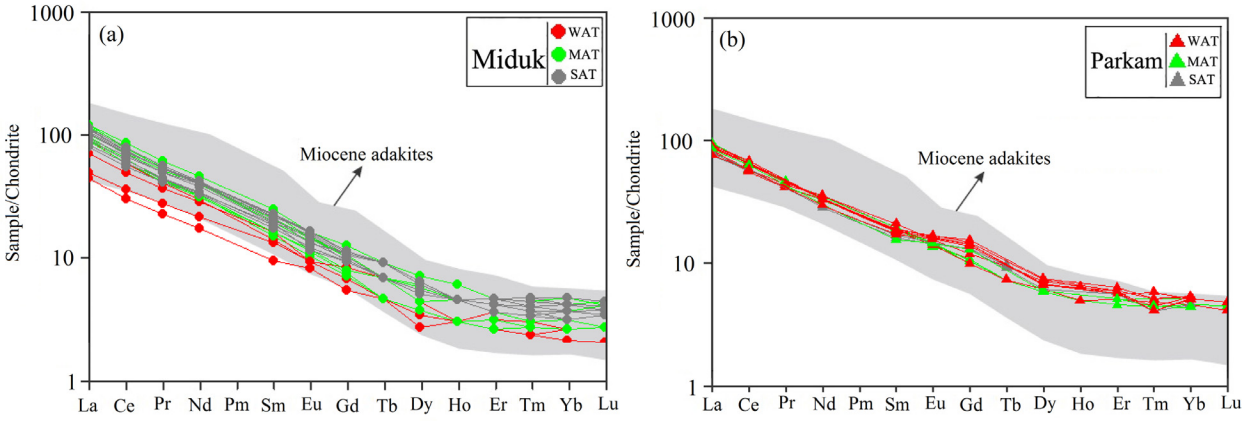

Fig. 14. Chondrite normalized REE for representative samples from-Meiduk (a) and Parkam (b) porphyry granitoids and their comparison with Miocene adakite-like high Sr/Y rocks in south Tibet (Li et al., 2011). The normalizing values are from Boynton, 1984.

Therefore, considering the absence of subduction system at Neogene time in the Dehaj-Sarduiyeh volcano-sedimentary belt (e.g. Qu et al., 2004; Hou et al., 2004; Jahangiri, 2007), the formation of MPGS can be related to the emplacement of their parental magma in the lower part of thickened continental crust (Fig. 16).

Dargahi (2007) for the first time reported the adakitic signature of Miocene Kuh-Panj type granitoids in the NW of Dehaj-Sarduiyeh volcano-sedimentary belt in the Sarcheshmeh area (Fig. 1). She considered their formation to Neogene adakitic magmatism in a post-collisional tectonic setting, after collision of Arabian–Eurasian in the Late Eocene. This argument can be considered for MPGS by

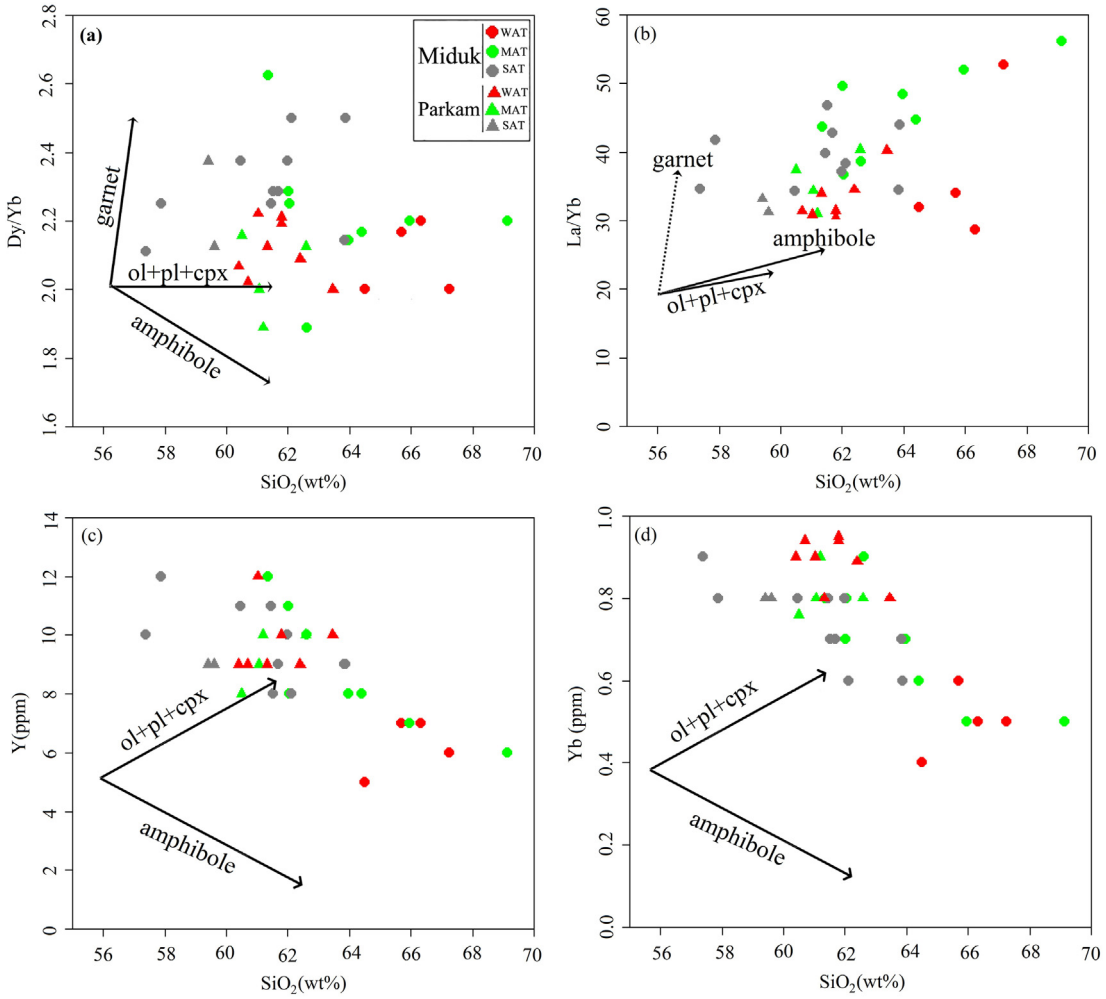

Fig. 15. Variation of (a) Dy/Yb versus SiO_2, (b) La/Yb versus SiO_2, (c) Y versus SiO_2 and (d) Yb versus SiO_2 diagrams from Lu et al., 2013 and 2015. These diagram indicates that amphibole fractionation played a significant role in the evolution of MPGS. Ol = Olivine, pl = Plagioclase, cpx = Clinopyroxene.

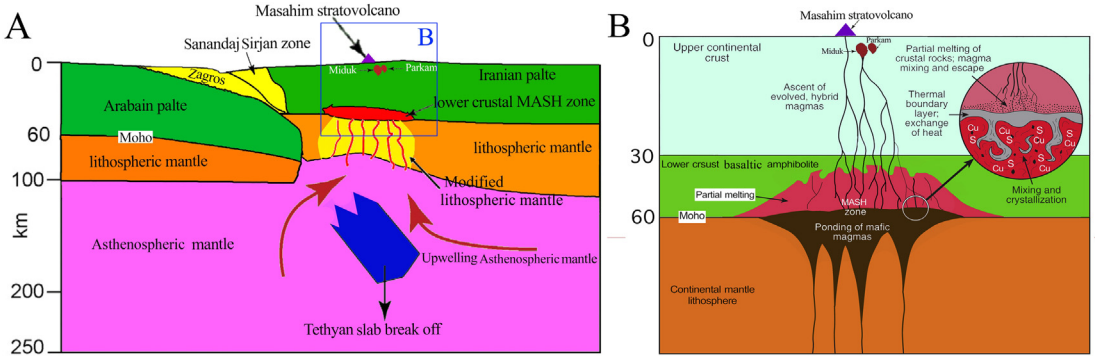

Fig. 16. Model of magmatic system responsible for formation of MPGS; A- Interaction between collisional mantle-derived mafic, hydrous melts and thickened mafic lower crustal rocks in a MASH process and associated adakitic porphyry Cu mineralization in MPGS at post-collisional tectonic setting in the Dehaj-Sarduiyeh volcano-sedimentary belt, south east extension of Urumieh-Dukhtar magmatic belt (Modified after Wang et al., 2015). B- The emplacement of mantle derived basaltic melt at the base of the thickened continental crust and its conversion to basaltic amphibolite rock due to compressional stress increase and tectonic shortening (Modified after Richards, 2003). In the post-collisional tectonic settings the partial melting of lithospheric mantle could take place due to the rising of hot asthenospheric mantle through the break-off of the subducted oceanic slab. The ascent of this hydrous, intermediate and oxidizing melt at shallow crustal levels formed the MPGS, during Neogene crustal thickening, in the Middle Miocene.

referring to tectonic setting diagrams in Figs. 10 and 11. This is also consistent with the final stage of post-collisional tectono-magmatic evolution of the UDMA and its south-eastern extension (Dehaj-Sarduiyeh volcano-sedimentary belt in Kerman) (Dargahi, 2007) in the Middle Miocene in an active continental margin.

Dehydration melting of basaltic amphibolites do not produce melts that dissolved H_2O to match the high H_2O contents (>10 wt %) of the copper ore–forming magmas (Lu et al., 2015). Therefore, the MPGS cannot be produced by dehydration melting of basaltic amphibolites in a thickened continental crust The positive correlation between La/Yb and SiO_2, and negative correlation between Dy/Yb (especially for Parkam granitoid), Y, Yb and SiO_2 (Fig. 15), all suggest that amphibole fractionation played a significant role in the genesis of Meiduk and Parkam adakite-like granitoids (Loucks, 2014; Lu et al., 2013, 2015). This together with the high La/Yb (≥20) and Sr/Y > 40 ratios clearly show that the MPGS were derived by high-pressure differentiation involving amphibole and magma mixing of hydrous mafic magmas under variable conditions of PH_2O with no plagioclase remaining in the residual phase (Lu et al., 2015). We suggest that the MPGS are residually H_2O-enriched, high-pressure differentiation products of hydrous mafic partial melts of mantle wedge.

Furthermore, it has been pointed out that the adakites resulted from melting of subducted oceanic crust have Mg# of 58–72 and low content Rb/Sr ratio of 0.01–0.04 ppm (Drummond et al., 1996; Rapp and Watson, 1995). In contrast, adakites formed by the melting of thickened lower continental crust have Rb/Sr ratio > 0.05 ppm and Mg#27–54 (Drummond et al., 1996; Hou et al., 2004). Thus, the Rb/Sr ratio of 0.04–0.7 ppm and Mg#27.1–49.5 in the MPGS also point to their formation in the thickened lower continental crust from a basaltic composition that was formed by the partial melting of lithospheric mantle due to the upwelling of hot asthenospheric mantle through the break-off of the subducted oceanic slab in the post-collisional tectonic setting (Daves and Blanckenburg, 1995; Haschke and Ben-Avraham, 2005). The basaltic melt pond at the base of the thickened continental crust at the depth of >40 km where an increase in compressional stress and tectonic shortening caused its conversion to a basaltic amphibolite (Rapp et al., 1999; Lentz, 1998; Sillitoe, 1998; Cooke et al., 2005; Lu et al., 2015). As a result, a zone of MASH was created at the boundary of the thickened continental crust and lithospheric mantle, which was ultimately responsible for the formation of intermediate to felsic adakitic like magma. Intrusion of this hydrous, intermediate and oxidizing magma ($Eu/Eu^* \geq 1$) at the shallow crustal levels (2–3 km) (Burnham, 1981) has generated MPGS (Fig. 16) with adakitic like geochemical affinity such as depletion in HREE, high Sr and to some extent high MgO. Having said that, the mantle-derived hydrous magmas could provide large quantities of heat and water which can facilitates partial melting and assimilation of lowermost crustal rocks (Burnham, 1981; Yang et al., 2015). Moreover, additional water can be induced into the system by amphibole breakdown due to increasing pressure at the lower crust during crustal thickening (Kay, 2001). Petford and Atherton (1993) also believe that the increase in geothermal gradient as a result of crustal thickening may also upsurge the temperature in the lithospheric mantle and cause its subsequent partial melting.

The Sr isotopic compositions of the Meiduk porphyry copper deposit characterized by a narrow range of initial $^{87}Sr/^{86}Sr$ (I_{Sr}) ratios (0.70455) (Hassanzadeh, 1993). Haschke et al. (2010) argued that lower I_{Sr} ratios of productive porphyries generally reflect mantle source affinities or a deep-crustal mafic source with amphibole and/or garnet as source minerals. The lowest I_{sr} ratios of the Meiduk porphyry copper deposit, indicating that MPGS have not been generated through a combined shallow crustal assimilation (Castillo et al., 1999).

Likewise, in many post-subductional collision settings such as MPGS, re-melting of sulphide-bearing lower crustal rocks under sulphur unsaturated conditions can led to dissolving of sulphides and their metals and likely development of post-subductional porphyry Cu ± Au deposits (Richards, 2015). Also, by considering the tectonic setting of MPGS, the role of two parameters of intensive oxidation state and extensive sulphur content should be considered on the behavior of metals during partial melting in the mantle, differentiation in the lower thickened crust, and during volatile exsolution and cooling (Fig. 16) (Burnham, 1979; Candela, 1992; Richards, 2011, 2015).

9. Conclusions

The Middle Miocene Meiduk and Parkam porphyry granitic stocks, located in the southeastern part of the UDMA, belong to the Kuh-Panj type granitoids. The main mineralization phases of the MPGS are hosted by quartz diorite, granodiorite and diorite with porphyritic and occasionally inequi-microgranular textures. The whole rock geochemical analysis indicates calc-alkaline, metaluminous to weakly peraluminous and I-type nature for the MPGS. Their geochemical characteristics such as typical Al_2O_3 contents,

high Sr, low Yb, strongly differentiated REE patterns, and lack of Eu anomaly indicate an adakitic like signatures. Geochemical data also suggest that the MPGS formed in a post-collisional tectonic setting after continental collision between the Arabian and Iranian plates at the final evolution stage of the UDMA and its south-eastern extension (Dehaj-Sarduiyeh volcano-sedimentary belt). We suggest that the MPGS are residually H_2O-enriched, high-pressure differentiation products of hydrous mafic partial melts of lithospheric mantle. Its melting probably occurred as a consequence of slab break-off and upwelling of the hot asthenospheric mantle. As a result, a zone of melting-assimilation-storage and homogenization (MASH) has been created near the boundary between lower parts of thickened continental crust-lithospheric mantle which was eventually responsible for the formation of intermediate to felsic adakitic like magma. The intrusion of this hydrous, intermediate and oxidizing ($Eu/Eu^* = 0.79–1.13$) magma at shallow crustal levels (2–3 km) have generated MPGS. The compressional conditions and oxidized nature of adakitic magma resulted by dissolving of large amounts of sulphide in the source region and adding it into the melt, transferring of sulphide phases in magma and preventing the separation of sulphide phases from intermediate-acidic melt. The ascent of this hydrous, oxidized, sulphur and metal rich magma and its emplacement into shallow depth in the crust has formed the MPGS porphyry copper deposits.

Acknowledgements

We would like to thank the Shahid Bahonar University of Kerman and National Iranian Copper Industries Company (NICICO) for their financial supports. We gratefully acknowledge Dr Ayati and Dr Yongjun Lu for their constructive and helpful reviews which have largely improved this manuscript. We also appreciate the very helpful suggestions and comments by the Editor-in-Chief Professor Franco Pirajno and Associate Editor Dr. Hooshang Asadi Haroni.

References

Agard, P., Omrani, J., Jolivet, L., Mouthereau, F., 2005. Convergence history across Zagros, Iran: constraints from collisional and earlier deformation. Int. J. Earth Sci. 94, 401–419.
Alavi, M., 1994. Tectonics of the Zagros orogenic belt of Iran: new data and interpretations. Tectonophysics 229, 211–238.
Alavi, M., 2004. Regional stratigraphy of the Zagros folded-thrust belt of Iran and its proforeland evolution. Am. J. Sci. 304, 1–20.
Alavi, M., 2007. Structure of the Zagros fold–thrust belt in Iran. Am. J. Sci. 307, 1064–1095.
Allen, M.B., Armstrong, H.A., 2008. Arabia-Eurasia collision and the forcing of mid Cenozoic global cooling. Palaeogeogr. Palaeocl. 265, 52–58.
Asadi, S., Moore, F., Zarasvandi, A., Khosrojerdi, M., 2013. First report on the occurrence of CO_2-bearing fluid inclusions in the Meiduk porphyry copper deposit, Iran: implications for mineralization processes in a continental collision setting. Geologos 19, 301–320.
Asadi, H.H., Porwal, A., Fatehi, M., Kianpouryan, S., Lu, Y.J., 2015. Exploration feature selection applied to hybrid data integration modeling: targeting copper-gold potential in central Iran. Ore Geol. Rev. 71, 819–838.
Atherton, M.P., Petford, N., 1993. Generation of sodium rich magmas from newly underplated basaltic crust. Nature 362, 144–146.
Batchelor, R.A., Bowden, P., 1985. Petrographic interpretation of granitoid rocks using multicationic parameters. Chemical Geology 48, 43–55.
Berberian, M., King, G.C., 1981. Towards a paleogeography and tectonic evolution of Iran. Can. J. Earth Sci. 18, 210–265.
Berberian, F., Muir, I.D., Pankhurst, R.J., Berberian, M., 1982. Late Cretaceous and early Miocene Andean-type plutonic activity in northern Makran and central Iran. J. Geol. Sci. 139, 605–614.
Beydoun, Z.R., Hughes Clarke, M.W., Stoneley, R., 1992. A late Tertiary foreland basin overprinted onto the outer edge of a vast hydrocarbon-rich Paleozoic-Mesozoic passive-margin shelf. In: Macqueen, R.W., Leckie, D.A. (Eds.). Foreland Basins and Fold Belts, Petroleum in the Zagros Basin: American Association of Petroleum Geologist Memoir. 55, 309–339.
Boynton, W.V., 1984. Cosmochemistry of the rare earth elements: meteorite studies. In: Henderson, P. (Ed.), Rare Earth Element Geochem.. Elsevier, Amsterdam, pp. 63–114.
Burnham, C.W., 1979. Magmas and hydrothermal fluids. In: Banes, H.L. (Ed.), Geochemistry of Hydrothermal Ore Deposit. second ed. John Wiley and Sons, New York, pp. 71–136.
Burnham, C.W., 1981. Convergence and mineralization — is there a relation? Geol. Soc. America. Memoir. 154, 761–768.
Candela, P.A., 1992. Controls on ore metal ratios in granite-related ore systems: An experimental and computational approach. T. Roy. Soc. Edin-Earth Sci. 83, 317–326.
Castillo, P.R., Janney, P.E., Solidum, R.U., 1999. Petrology and geochemistry of Camiguin Island, southern Philippines: insights to the source of adakites and other lavas in a complex arc setting. Contrib. Mineral. Petr. 134, 33–51.
Condie, K.C., 1989. Geochemical changes in basalts and andesites across the Archean-Proterozoic boundary: identification and significance. Lithos 23, 1–18.
Cooke, D.R., Hollings, P., Walshe, J.L., 2005. Giant porphyry deposits: characteristics, distribution, and tectonic controls. Econ. Geol. 100, 801–818.
Cox, K.G., Bell, J.D., Pankhurst, R.J., 1979. The interpration of igneous rocks. George, Allen and Unwine, Londone.
Dargahi, S., 2007. Post-collisional Miocene magmatism in the Sarcheshmeh-Shahr-e-Babak region, NW of Kerman: Isotopic study, petrogenetic analysis and geodynamic pattern of granitoid intrusives and the role of adakitic magmatism in development of copper mineralization (Unpublished Ph.D. thesis). Shahid Bahonar University of Kerman, in Persian. 310 pp.
Daves, J.H., Blanckenburg, V.F., 1995. Slab break off: a model of lithosphere detachment and its test in the magmatism and deformation of collisional orogenes. Earth Planet. Sci. Lett. 129, 85–102.
Defant, M.J., Drummond, M.S., 1990. Derivation of some modern magmas by melting of young subducted lithosphere. Nature 347, 662–665.
Dehghani, G.A., Makris, T., 1983. The gravity field and crustal structure of Iran. Geodynamic project (Geotraverse) in Iran. Geol. Survey Iran 51, 50–68. Final Report number.
Delaroche, H., Leterrier, J., Grandclaude, P., Marchal, M., 1980. A classification of volcanic and plutonic rocks using R1R2-diagram and major-element analyses–its relationships with current nomenclature. Chem. Geol. 29, 183–210.
Drummond, M.S., Defant, M.J., Kepezhinskas, P.K., 1996. Petrogenesis of slab-derived trondhjemite–tonalite–dacite/adakite magmas. Trans. Royal Soc. Edinburgh: Earth Sci. 87 (1–2), 205–215.
Green, N.L., Harry, D.L., 1999. On the relationship between subducted slab age and arc basalt petrogenesis, Cascadia subduction system, North America. Earth Planet. Sci. Lett. 171, 367–381.
Han, C., Xiao, W., Zhao, G., Mao, J., Yang, J., Wang, Z., Yan, Z., Mao, Q., 2006. Geological characteristics and genesis of the Tuwu porphyry copper deposit, Hami, Xinjiang, central Asia. Ore Geol. Rev. 29, 77–94.
Harris, N.B.W., Pearce, J.A., Tindle, A.G., 1986. Geochemical characteristics of collision-zone magmatism. In: Coward, M.P., Ries, A.C. (Eds.). Collision Tectonics. Geological Society of London, Special Publication. 19, 67–81.
Haschke, M.R., Ben-Avraham, Z., 2005. Adakites from collision- modified lithosphere. Geophys. Res. Lett. 32, L15302. doi:10.1029.
Haschke, M., Ahmadian, J., Murata, M., McDonald, I., 2010. Copper mineralization prevented by arc-root delamination during Alpine-Himalayan collision in Central Iran. Econ. Geol. 105, 855–865.
Hassanzadeh, J., 1993. Metallogenic and tectono-magmatic events in SE sector of the Cenozoic active continental margin of Central Iran (Shahr-e-Babak, Kerman Province) (Ph.D. Thesis). University of California, Los Angeles, 201p.
Hempton, M.R., 1987. Constraints on Arabian plate motion and extensional history of the Red Sea. Tectonics 6, 687–705.
Hikov, A., 2013. Geochemistry of hydrothermally altered rocks from the Asarel porphyry copper deposit, Central Srednogorie. Geologica Balcanica 42, 3–28.
Horton, B.K., Hassanzadeh, J., Stockli, D.F., Axen, G.J., Gillis, R.J., Guest, B., Amini, A., 2008. Detrital zircon provenance of Neoproterozoic to Cenozoic deposits in Iran: implications for chrono stratigraphy and collisional tectonics. Tectonophysics 451, 97–122.
Hou, Z.-Q., Gao, Y.-F., Qu, X.M., Rui, Z.-Y., Mo, X.-X., 2004. Origin of adakitic intrusives generated during mid-Miocene east-west extension in southern Tibet. Earth Planet. Sci. Lett. 220, 139–155.
Hou, Z.Q., Duan, L.F., Lu, Y.J., Zheng, Y.C., Zhu, D.C., Yang, Z.M., Yang, Z.S., Wang, B.D., Pei, Y.R., Zhao, Z.D., McCuaig, T.C., 2015a. Lithospheric architecture of the Lhasa Terrane and its control on ore deposits in the Himalayan-Tibetan orogen. Econ. Geol. 110, 1541–1575.
Hou, Z.Q., Yang, Z.M., Lu, Y.J., Kemp, A.I.S., Zheng, Y.C., Li, Q.Y., Tang, J.X., Yang, Z.S., Duan, L.F., 2015b. A genetic linkage between subduction- and collision-related porphyry Cu deposits in continental collision zones. Geology 43, 247–250.
İmer, A., Richards, J.P., Creaser, R.A., 2014. The late Oligocene Cevizlidere Cu-Au-Mo deposit, Tunceli Province, eastern Turkey. Mineral Deposita. http://dx.doi.org/10.1007/s00126-014-0533-4/.
Jahangiri, A., 2007. Post-collisional Miocene adakitic volcanism in NW Iran: geochemical and geodynamic implications. J. Asian Earth Sci. 30, 433–447.
Kay, R.W., 1987. Aleutian magnesian andesites: melts from subducted Pacific Ocean crust. J. Volcanol. Geoth. Res. 4, 117–132.
Kay, S.M., Mpodozis, C., 2002. Magmatism as a probe to the Neogene shallowing of the Nazca of the Nazca plate beneath the modern Chilean flat-slab. J. S. Am. Earth Sci. 15, 39–57.
Kay, S.M., Mpodozis, C., 2001. Central Andes ore deposits linked to evolving shallow subduction systems and thickening crust. Geol. Soc. Am. 11, 4–9.
Kay, S.M., Maksaev, V., Mpodozis, C., Moscoso, R., Nasi, C., 1987. Probing the evolving Andean lithosphere: Mid-Late Tertiary magmatism in Chile (29–30.5°S) over the zone of subhorizontal subduction. J. Geophys. Res. 92, 6183–6189.

Kay, S.M., Mpodozis, C., Ramos, V.A., Munizaga, F., 1991. Magmasource variations for mid-late Tertiary magmatic rocks associated with a shallow in subduction zone and a thickening crust in the central Andes (28–33°S). In: Harmon, R.S., and Rapela, C.W., (Eds.). Andean magmatism and its tectonic setting. Geological Society of America Special Paper. 265, 113–137.
Kogiso, T., Tatsumi, Y., Nakano, S., 1997. Trace element transport during dehydration processes in the subducted crust: 1. Experiments and implications for the origin of ocean island basalts. Earth Planet. Sci. Lett. 148, 193–205.
Lameyre, J., Bowden, P., 1982. Plutonic rock series: Discrimination of various granitoid series and related rocks. Journal of Volcanology and Geothermal Research 14, 169–186.
Lentz, D.R., 1998. Petrogenetic and geodynamic implications of extensional regimes in the Phanerozoic subduction zones and their relationship to VMS-forming systems. Ore Geol. Rev. 12, 289–327.
Li, J.X., Qin, K.Z., Li, G.M., Xiao, B., Chen, L., Zhao, J.X., 2011. Post-collisional ore-bearing adakitic porphyries from Gangdese porphyry copper belt, southern Tibet. Meltingof thickened juvenile arc lower crust. Lithos 126, 264–277.
Loucks, R.R., 2014. Distinctive composition of copper-ore-forming arc magmas. Austral. J. Earth Sci. 61, 5–16.
Lu, Y.J., Loucks, R.R., Fiorentini, M.L., 2013. Genesis of fertile hydrous adakite-like melts in post-subduction porphyry Cu systems of Tibet. 12th SGA Biennial Meeting, 12–15 August 2013, Uppsala, Sweden. Proceedings. 3, 1443-1446.
Lu, Y.J., Loucks, R.R., Fiorentini, M.L., Yang, Z.M., Hou, Z.Q., 2015. Fluid flux melting generated post-collisional high-Sr/Y copper-ore–forming water-rich magmas in Tibet. Geology 43, 583–586.
Lu, Y.J., Loucks, R.R., Fiorentini, M.L., Mc Cuaig, T.C., Evans, N.J., Yang, Z.M., Hou, Z.Q., Kirkland, C.L., Parra-Avila, L.A., Kobussen, A., 2016. Zircon compositions as a pathfinder for porphyry Cu ± Mo ± Au deposits. Soc. Econ. Geol. Spec. Publ. 19, 329–347.
MacLean, W.H., Barrett, T.J., 1993. Lithochemical techniques using immobile elements. J. Geochem. Explor. 48, 109–133.
Maniar, P.D., Piccoli, P.M., 1989. Tectonic discrimination of granitoids. Geol. Soc. Am. Bull. 101, 635–643.
Martin, H., 1999. Adakitic magmas: modern analogues of Archaean granitoids. Lithos 46, 411–429.
Martina, H., Smithies, R.H., Rapp, R., Moyen, J.F., Champion, D., 2005. An overview of adakite, tonalite–trondhjemite–granodiorite (TTG), and sanukitoid: relationships and some implications for crustal evolution. Lithos 79, 1–24.
McInnes, B.I.A., Evans, N.J., Belousova, E., Griffin, W.T., Andrew, R.L., 2003. Timing of mineralization and exhumation processes at the Sarcheshmeh and Meiduk porphyry Cu deposits, Kerman belt, Iran: Mineral exploration and sustainable development, Eliopoulos et al. ((Eds.). Millpress, Roterdam, 1197–1200, ISBN 9077017 77 1.
Mohajjel, M., Fergusson, C., 2000. Dextral transgression in Late Cretaceous continental collision zone. western Iran. J. Struct. Geol. 22, 1125–1139.
Mohajjel, M., Fergusson, C.L., Sahandi, M.R., 2003. Cretaceous-Tertiary convergence and continental collision, Sanandaj-Sirjan zone, western Iran. J. Asian Earth Sci. 21, 397–412.
Mohamadi Laghab, M., 2011. Study of alteration mineralization haloes and distribution pattern presenting of valuable element Cu, Mo, Au, Ag in Sara porphyry copper deposit (M.Sc. Thesis). Damghan University School of Earth Sciences, Kerman province, 229 p.
Mungall, J.E., 2002. Roasting the mantle: slab melting and the genesis of major Au and Au-rich Cu deposits. Geology 30, 915–918.
Outomec, 1992. Techno-economic feasibility study and relevant backing technical studies of Miduk Copper Project. Outokumpu, Finland. 171p.
Oyarzun, R., Marquez, A., Lillo, Y., Lopez, I., River, S., 2001. Giant versus small porphyry copper deposits of Cenozoic age northern Chile: adakitic versus normal calc-alkaline magmatism. Miner. Deposita 36, 794–798.
Ozdemir, Y., 2011. Volcanostratigraphy and petrogenesis of Suphan stratovolcano. (Ph.D. thesis). Middle East Technical University, Ankara, Turkey.
Pearce, J.A., 1996. Sources and settings of granitic rocks. Episodes 19, 120–125.
Pearce, J.A., Harris, N.B.W., Tindle, A.G., 1984. Trace element discrimination diagrams for the tectonic interpretation of granitic rocks. J. Petrol. 25, 956–983.
Pearce, J.A., Bender, J.F., De Long, S.E., Kidd, W.S.F., Low, P.J., Güner, Y., Saroğlu, F., Yılmaz, Y., Moorbath, S., Mitchell, J.J., 1990. Genesis of collision volcanism in eastern Anatolia Turkey. J. Volcanol. Geoth. Res. 44, 189–229.
Peccerillo, A., Taylor, S.R., 1976. Geochemistry of Eocene calc-alkaline volcanic rocks from the Kastamonu area, northern Turkey. Contrib. Mineral. Petrol. 58, 63–81.
Petford, N., Atherton, M., 1996. Na-rich partial melts from newly underplated basaltic crust: the Cordillera Blanca Batholith, Peru. J. Petrol. 37, 1491–1521.
Pirajno, F., 2009, "Hydrothermal Processes and Mineral Systems", Springer, 1273 p.
Prouteau, G., Scaillet, B., Pichavant, M., Maury, R.C., 1999. Fluid- present melting of ocean crust in subduction zones. Geology 27, 1111–1114.
Qu, X.M., Hou, Z.Q., Li, Y.G., 2004. Melt components derived from a subducted slab in late orogenic ore-bearing porphyries in the Gangdese copper belt, southern Tibetan plateau. Lithos 74, 131–148.
Rapp, R.P., Watson, E.B., 1995. Dehydration melting of meta basalt at 8–32 kbar: implications for continental growth and crust-mantle recycling. J. Petrol. 36, 891–931.
Rapp, R.P., Shimizu, N., Norman, M.D., Applegate, G.S., 1999. Reaction between slab-derived melts and peridotite in the mantle wedge: experimental constraints at 38 GPa. Chem. Geol. 160, 335–356.
Reich, M., Parada, M.A., Palacios, C., Dietrich, A., Schultz, F., Lehmann, B., 2003. Adakite-like signature of late Miocene intrusions at the Los Pelambres giant porphyry copper deposit in the Andes of central Chile: metallogenic implications. Mineralium Deposita 38, 876–885.
Richards, J.P., 2003. Tectono-magmatic precursors for porphyry Cu- (Mo-Au) deposit formation. Econ. Geol. 98, 1515–1533.
Richards, J.P., 2011. Magmatic to hydrothermal metal fluxes in convergent and collided margins. Ore Geol. Rev. 40 (1), 1–26.
Richards, J.P., 2015. The oxidation state, and sulfur and Cu contents of arc magmas: implications for metallogeny. Lithos 233, 27–45.
Richards, J.P., Kerrich, R., 2007. Adakite-like rocks: their diverse origins and questionable role in metallogenesis. Econ. Geol. 102, 537–576.
Richards, J.R., 2009. Postsubduction porphyry Cu–Au and epithermal Au deposits: products of remelting of subduction-modified lithosphere. Geology 37, 247–250.
Ricou, L.E., 1994. Tethys reconstructed: plates continental fragments and their boundaries since 260 Ma from Central America to south-eastern Asia. Geodin. Acta 7, 169–218.
Rohrlach, B.D., Loucks, R.R., 2005. Multimillion-year cyclic ramp-up of volatiles in a lower crustal magma reservoir trapped below the Tampakan copper-gold deposit by Mio-Pliocene crustal compression in the southern Philippines. In: Porter, T.M. (Ed.), Super Porphyry Copper & Gold Deposits A Global Perspective, Adelaide, vol. 2. PCG Publishing, Australia, pp. 369–407.
Saric, A., Djordjevic, M., Dimitrijevic, M.N., 1971. Geological Map of Shahr-E-Babak, Scale 1/100000. Geological Survey of Iran, Tehran, Iran.
Shahabpour, J., 2000. Behaviour of Cu and Mo in the SarCheshmeh porphyry Cu deposit, Kerman, Iran. CIM Bull. 93, 44–51.
Sillitoe, R.H., 1998. Major regional factors favouring large size, high hypogene grade, elevated gold content and supergene oxidation and enrichment of porphyry copper deposits. In: Porter, T.M. (Ed.), Porphyry and Hydrothermal Copper and Gold Deposits: A Global Perspective. Australian Mineral Foundation Publishing Inc, Adelaide, pp. 21–34.
Stern, C.R.,Skewes, M. A., 2005. Origin of giant Miocene and Pliocene Cu-Mo deposits in central Chile: role of ridge subduction, decreased abduction angle, subduction erosion, crustal thickening and long- lived batholite size, open system magma chambers, Super porphyry copper and Gold Deposits – A Global perspective. PGC Publishing, Adelaid1, 65-82.
Sun, S.S., McDonough, W.F., 1989. Chemical and isotopic systematics of oceanic basalts; implications for mantle composition and processes. In: Saunders, A.D., Norry, M.J. (Eds.). Magmatism in the ocean basins. Geological Society Special Publications. 42, 313–345.
Waight, T.E., Weaver, S.D., Muir, R.J., 1998. The Hohonu Batholith of North Westland, New Zealand: granitoid compositions controlled by source H_2O contents and generated during tectonic transition. Contrib. Mineral. Petrol. 130, 225–239.
Wang, Q., Xu, J.F., Jian, P., Bao, Z.W., Zhao, Z.H., Li, C.F., Xiong, X.L., Ma, J.L., 2006. Petrogenesis of adakitic porphyries in an extensional tectonic setting, Dexing, South China: implications for the genesis of porphyry copper mineralization. J. Petrol. 47, 119–144.
Wang, R., Richards, J.P., Hou, Z.Q., An, F., Creaser, A.R., 2015. Zircon U-Pb age and Sr–Nd–Hf–O isotope geochemistry of the Paleocene-Eocene igneous rocks in western Gangdese: evidence for the timing of Neo-Tethyan slab break off. Lithos 224–225, 179–194.
Whattam, S.A., Montes, C., McFadden, R.R., Cardona, A., Ramirez, D., Valencia, V., 2012. Age and origion of earliest adakitic-like magmatism in Panama: implication for the tectonic evolution of the Panamanian magmatic arc system. Lithos 142, 226–244.
Winchester, J.A., Floyd, P.A., 1977. Geochemical discrimination of different magma series and their differentiation products using immobile elements. Chem. Geol. 20, 325–343.
Yang, Z.M., Lu, Y.J., Hou, Z.Q., Chang, Z.S., 2015. High-Mg Diorite from Qulong in Southern Tibet: implications for the Genesis of Adakite-like Intrusions and Associated Porphyry Cu Deposits in Collisional Orogens. J. Petrol. 56, 227–254.
Zen, E.AN., 1986. Aluminum enrichment in silicate melts by fractional crystallization: some mineralogical and petrographic constraints. J. Petrol. 27, 1095–1118.
Zhu, D.C., Zhao, Z.D., Pan, G.T., Lee, H.Y., Kang, Z.Q., Liao, Z.L., Wang, L.Q., Li, G.M., Dong, G.C., Liu, B., 2009. Early cretaceous subduction-related adakite-like rocks of the Gangdese Belt, southern Tibet: products of slab melting and subsequent melt peridotite interaction? J. Asian Earth Sci. 34, 298–309.